Tetrameric UvrD helicase is located at the *E. coli* replisome due to frequent replication blocks

Adam J. M Wollman[1,2,3], Aisha H. Syeda[1,2], Jamieson A. L. Howard[1,2], Alex Payne-Dwyer[1,2], Andrew Leech[4] , Colin Guy[5, 6], Peter McGlynn[2,6], Michelle Hawkins[2] and Mark C. Leake[1,2]

The authors wish it to be known that, in their opinion, the first two authors should be regarded as joint First Authors

[1] School of Physics, Engineering and Technology, University of York, York YO10 5DD, United Kingdom.

[2] Department of Biology, University of York, York YO10 5DD, United Kingdom.

[3] Current address: Biosciences Institute, Newcastle University, NE1 7RU, United Kingdom.

[4] Bioscience Technology Facility, Department of Biology, University of York, York YO10 5DD, United Kingdom

[5] Current address: Covance Laboratories Ltd., Otley Road, Harrogate, HG3 1PY, United Kingdom

[6] Previous address: School of Medical Sciences, Institute of Medical Sciences, University of Aberdeen, Foresterhill, Aberdeen AB25 2ZD, United Kingdom

* To whom correspondence should be addressed. To whom correspondence should be addressed. Tel: +44 (0)1904322697. Email: mark.leake@york.ac.uk

Present Address: School of Physics, Engineering and Technology, and Department of Biology, University of York, York YO10 5DD, United Kingdom

ABSTRACT

DNA replication in all organisms must overcome nucleoprotein blocks to complete genome duplication. Accessory replicative helicases in *Escherichia coli*, Rep and UvrD, help replication machinery overcome blocks by removing incoming nucleoprotein complexes or aiding the re-initiation of replication. Mechanistic details of Rep function have emerged from recent live cell studies, however, the multiple activities of UvrD in DNA repair and its roles as an accessory helicase in live cells remain unclear. Here, by integrating super-resolved single-molecule fluorescence microscopy with biochemical analysis, we find that UvrD self-associates into a tetramer and, unlike Rep, is not recruited to a specific replisome protein despite being found at approximately 80% of replication forks. Instead, its recruitment to forks is likely mediated by the very high frequency of replication blocks due to DNA bound proteins, including RNA polymerase and DNA damage. Deleting *rep* and DNA repair factor genes *mutS* and *uvrA*, and inhibiting transcription through RNA polymerase

mutation and antibiotic inhibition, indicates that the level of UvrD at the fork is dependent on its function. Our findings show that UvrD is recruited to sites of nucleoprotein blocks via distinctly different mechanisms to Rep and plays a multi-faceted role in ensuring successful DNA replication.

INTRODUCTION

Replication and transcription of DNA occur simultaneously in *Escherichia coli,* making conflicts between the bacterial replisome, the molecular replication machine comprising in excess of 10 different proteins, and RNA polymerase (RNAP) inevitable (1–4). Collisions between the replication and transcription machineries hinder replication fork progression and cause genome instability (5–14). RNAP can pause, stall and backtrack while actively transcribing, and any immobile RNAP molecules present long-lived barriers to replisomes (15, 16). These factors make RNAP the most common nucleoprotein obstacle for translocating replisomes. DNA is also frequently damaged in normal growth conditions due to exposure to endogenous and exogenous DNA damaging agents. The resulting DNA damage also presents significant obstacles for normal replication (17–19).

Several mechanisms exist to reduce conflict between the replisome and obstacles such as transcribing RNAPs. For example, transcription elongation and termination factors reduce the number of immobile RNA polymerases on DNA (1, 18, 20–24). Head-on collisions were originally thought to be more harmful (25–27) and therefore more important to resolve; a view supported by the occurrence of highly transcribed genes encoded on the leading strand, presumably to ensure co-directional transcription and replication (26, 28, 29). However, co-directional collisions of the replisome and transcription machinery also impact replication fork progression (3, 18, 30).

Accessory replicative helicases promote fork movement through nucleoprotein barriers and have been identified in prokaryotes and eukaryotes (1, 12, 13, 31, 32). The Rep and UvrD accessory helicases in *E. coli*, as well as the Pif1 helicase in *Saccharomyces cerevisiae*, perform important roles in helping to clear nucleoprotein complexes (33). More recently, Pif1 has been proposed to be a general displacement helicase for replication bypass of protein blocks, a function similar to the Rep and UvrD helicases (34). These helicases can reduce replisome pausing at several types of

native transcription complexes observed in living cells (13, 22, 35), and several types of engineered nucleoprotein blocks in biochemical experiments *in vitro* (1, 31).

Rep is the primary accessory helicase in *E. coli*, however, UvrD can partially compensate for the absence of Rep *in vivo* and has been shown to promote replication through stalled transcription elongation complexes (1, 12, 13, 36, 37). UvrD is a superfamily 1 helicase that translocates 3'-5' along ssDNA. The ability of UvrD to compensate partially for the absence of Rep has been attributed to the high degree of homology between these two helicases and the abundance of UvrD inside cells (12, 21, 38–40). The role of UvrD in nucleotide excision repair along with UvrABC proteins as well as in methyl-directed mismatch repair along with the MutHLS proteins is well characterised (41–46). UvrD interacts directly with RNAP but the functional importance of this interaction has been unclear until recently (47–50). UvrD has been suggested to promote backtracking of stalled RNAP as a first step in transcription-coupled repair (50, 51); however, other studies argue against UvrD playing any role in coupling nucleotide excision repair to stalled transcription complexes (48, 49, 52–56).

Here, we combined state-of-the-art live cell imaging using single-molecule microscopy with advanced biochemical activity experiments *in vitro* to elucidate how UvrD resolves replicative blocks. We used super-resolved high-speed single-molecule fluorescence microscopy of mGFP-UvrD in live cells co-expressing a fork marker, DnaQ-mCherry, to reveal that 80% of DnaQ foci colocalise with UvrD. Stepwise photobleaching intensity analysis showed that UvrD is a tetramer *in vivo*, to be compared with earlier observations performed *in vitro* using analytical ultracentrifugation that found a mixture of UvrD dimers and tetramers (57). Surface plasmon resonance (SPR) measurements of UvrD in combination with each replisome component identified no specific replisome protein interaction partner that would explain replisome-UvrD colocalisation. Deletion of Rep, mismatch repair protein MutS and nucleotide excision repair protein UvrA, and disruption of transcription using either mutation of RNAP or antibiotic inhibition, significantly reduces the number of UvrD or level of observed colocalisation of UvrD with the fork. Coupled with *in vitro* block-dependent differences in UvrD replication promotion efficiency, we conclude that UvrD is located at the *E. coli* replisome due to its role in resolving frequent blocks to replication.

RESULTS

UvrD is present at the majority of replication forks

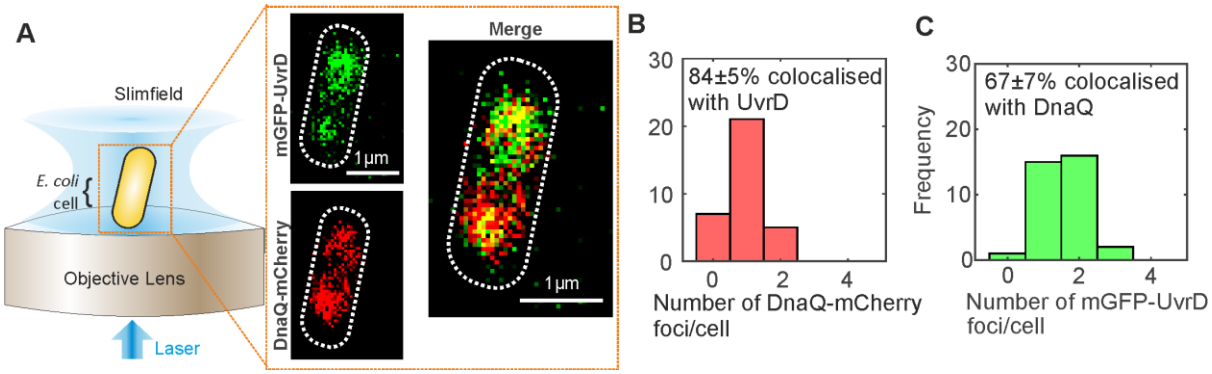

Figure 1: Super-resolved single-molecule light microscopy. (A). Slimfield microscope schematic and Slimfield micrographs of mGFP-UvrD, DnaQ-mCherry. (B) and (C) Histogram showing the number of DnaQ and UvrD foci detected per cell respectively, SD errors.

We investigated the role of UvrD in DNA replication using super-resolved single-molecule fluorescence microscopy to track dynamic patterns of fluorescently labelled UvrD localization relative to the replication fork in live cells (Figure 1A). We performed dual-colour Slimfield (63, 78) to assess the degree of colocalisation between UvrD and the replisome, using a similar imaging protocol as previously for Rep (13). We employed DnaQ-mCherry as a fork marker (13) along with a genomically integrated mGFP-UvrD fluorescent protein fusion construct to report on the localization of UvrD. DnaQ encodes the epsilon subunit, a core component of the DNA polymerase and is well established as a marker for the replication fork (13, 69, 79–81). These strains phenocopied the wild type strain for growth and in plasmid loss assays testing for mGFP-UvrD function retention (Supplementary Figures S1, S2, Tables S1-4). The helicase activity of mGFP-UvrD was comparable to the wild type enzyme in an *in vitro* unwinding assay (Supplementary Figure S3). Under Slimfield, we observed 1-2 DnaQ foci as in the previous study for Rep, corresponding to the two moving replication forks which appear as single foci near the start of replication when they are separated by less than the 200-300 nm diffraction limit of our microscope (Figure 1A,B Supplementary Figure S4). We also observed 1-2 UvrD foci per cell, of which 67 ± 7% (±SEM) were colocalised with DnaQ foci and 84 ± 5% of DnaQ foci were colocalised with UvrD (Figure 1B and C). We calculated the probability of random overlap between these foci, by modelling the nearest-neighbour foci separation as a Poisson distribution (70), to be 20%. To confirm that colocalisation between DnaQ and UvrD was not just a function of the nucleoid association of UvrD, we performed Slimfield

imaging of Heat-stable nucleoid-structuring protein (H-NS) tagged with GFP dual labelled with DnaQ-mCherry. H-NS associates with the nucleoid but not specifically with the fork. We found similar numbers of H-NS foci (Supplementary Figure S5) but only 38±4% DnaQ foci were colocalised with H-NS implying that, similarly to the Rep helicase (13), UvrD is present at the majority of replication forks.

UvrD is a tetramer in live bacterial cells

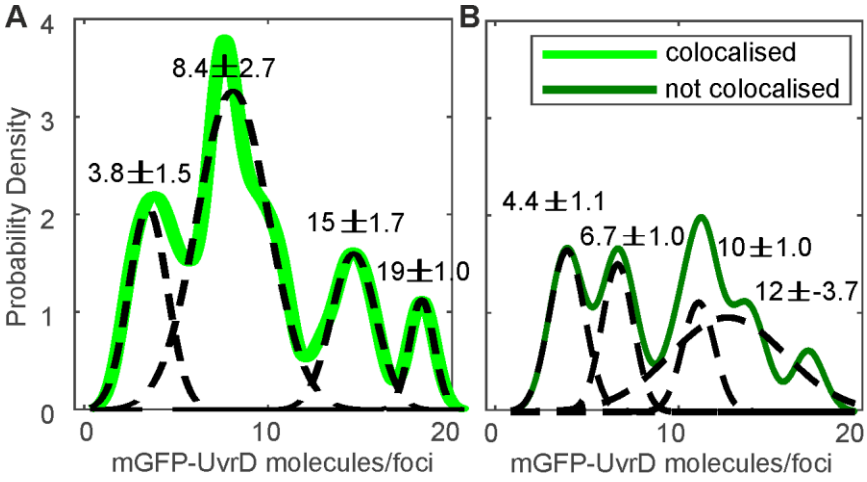

Figure 2 UvrD stoichiometry. The distribution of UvrD foci stoichiometry rendered as a kernel density estimate for foci colocalised (A) and not colocalised (B) with DnaQ foci. Distributions were fitted with multiple Gaussian peaks (black dotted lines) with the peak value ± error determined by the half width at half maximum indicated above each peak

Slimfield also enabled the stoichiometry of these foci to be determined by utilizing a method involving step-wise photobleaching analysis (69). Here, we determined the brightness of a single-molecule of mGFP or mCherry fluorescent protein under our Slimfield imaging conditions (Supplementary Figure S7), and used these values to normalize the initial brightness of all tracked foci as an estimate for the apparent stoichiometry in terms of number of fluorescently labelled molecules present. We found that DnaQ had the same range of 2-6 molecules per focus (Supplementary Figure S8) as we have found previously, corresponding to 2-3 polymerases per fork (13, 69). The distribution of the apparent stoichiometry of UvrD foci which are colocalised with DnaQ had a distinct lowest-order peak corresponding to approximately four molecules, with subsequent peaks at clear multiples of four (Figure 2A). UvrD foci that are not colocalised with DnaQ also contained a distinct lowest-order peak at four, but subsequent peaks were less clearly tetrameric. We performed

Size Exclusion Chromatography - Multi-Angle Laser Light Scattering (SEC-MALLS) to test whether the fluorescent protein labelling UvrD might be inducing multimers but found limited effects on UvrD assembly state, as expected from the K_D dissociation constant of fluorescent proteins containing the A206K mutation (82) (Supplementary Figure S9). UvrD has been shown to exist in a monomer-dimer-tetramer equilibrium *in vitro* (57). DNA unwinding experiments *in vitro* suggest UvrD must function as at least a dimer (83) or a trimer (84), however the oligomeric state of functional UvrD is disputed (reviewed in (85)). To our knowledge, these are the first UvrD stoichiometry measurements *in vivo* so we propose that UvrD forms a tetramer *in vivo* with multiple tetramers often at the replication fork. It should be noted that we often observe only a single DnaQ focus corresponding to two replication forks which are separated by less than the diffraction limit of our microscope (Supplementary Figure S8) such that some multiple tetramer UvrD foci correspond to two replication forks. The less distinct peaks in the UvrD foci that are not colocalised with DnaQ may indicate that other UvrD species (monomers, dimers or trimers) are also present.

We were also able to determine the total cell copy number of UvrD using a method which determined the total contribution of mGFP-UvrD fluorescence to the observed intensity in whole cells (72). We found approximately 800 molecules of UvrD per cell (Supplementary Figure S10), similar to that which we reported previously for Rep (13). This is a much lower level of UvrD than was reported using transcription rate measurements (86) or high-throughput proteomics (87) but is comparable to recent estimates using ribosome profiling (88).

No interaction partner was found for UvrD at the fork with SPR

Our earlier findings concerning the accessory helicase Rep indicated that colocalisation with the fork and recruitment to the replisome were mediated by specific interaction with the replicative helicase DnaB (89), with Rep and DnaB both exhibiting hexameric stoichiometry (13, 69). We sought to determine whether UvrD is also recruited by interacting with a specific replisome component using SPR on purified UvrD and each replisome component (Supplementary Figure 11). UvrD exhibited no direct interaction with primase, SSB, β sliding clamp, the DNA polymerase III αε, χψ or γ complexes; or θ, δ, δ′, χ, and γ subunits (12). We did initially identify a putative weak UvrD-Tau interaction. However, as a control we also tested Rep, and found this also interacted with Tau to a similar extent, and with ~100x lower affinity than UvrD

with known interaction partner UvrB (Supplementary Figure 8). We therefore conclude that the Tau interaction with UvrD is non-specific and that, unlike Rep, UvrD likely does not have a direct interaction partner at the replisome from the suite of replisome proteins tested. As UvrD is a tetramer at the replisome, it is also unlikely to be recruited by Rep, which has shown putative interaction (90).

UvrD presence at the replication fork is mediated by specific blocks to replication

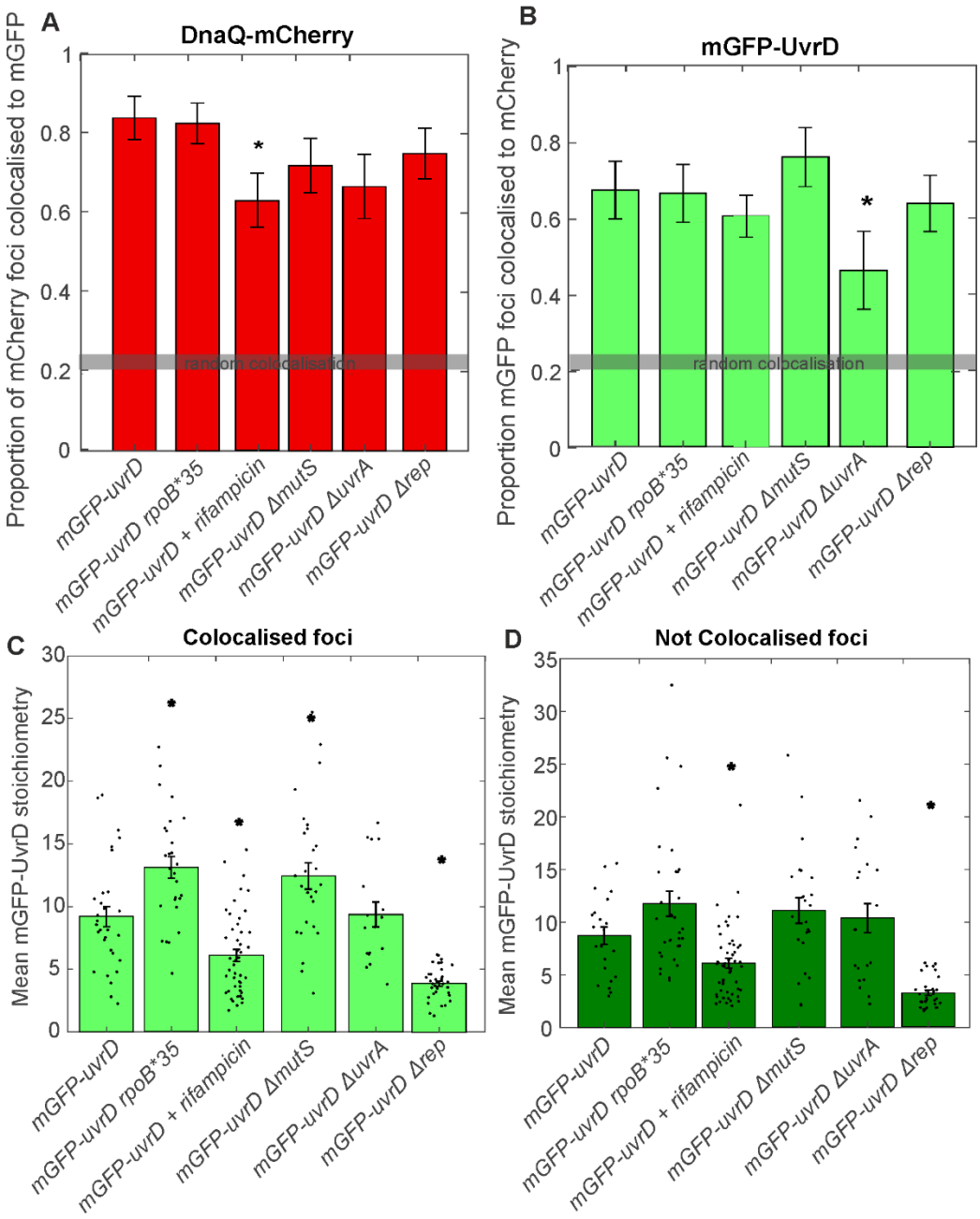

Figure 3: UvrD perturbations. A. and B. The mean proportion of colocalised DnaQ and UvrD foci per cell respectively. Error bars represent standard error in the mean and statistical

significance by Student's t-test $p<0.05$ indicated by *. C. and D. Jitter plots of colocalised and not colocalised UvrD stoichiometry respectively. Bars show mean UvrD stoichiometry with error bars showing the standard error in the mean and statistical significance by Student's t-tests $p<0.05$ indicated by *.

Since our SPR observations indicated that UvrD does not interact directly and specifically with any core replisome protein, we hypothesized that the association of UvrD with the replication fork might be dependent on its activity in resolving nucleoprotein blocks. To test this, we systematically impaired key DNA replication repair processes in which UvrD is implicated, as well as perturbing RNAP replicative blocks by disruption of transcription through both genetic mutation and antibiotic inhibition (Figure 3). We perturbed UvrD's activity in resolving DNA damage at replication blocks by deleting *mutS* or *uvrA*, rendering the strains defective in UvrD-associated mismatch repair or nucleotide excision repair respectively (43, 91). We reduced the need for UvrD to remove transcriptional blocks to replication (49) by introducing the *rpoB*35* mutation, which destabilizes open complexes formed during initiation of transcription (92, 93); and by using the antibiotic rifampicin, which blocks elongation of RNA transcripts (94). All of these strains were healthy under normal growth conditions (Supplementary Figure S1, Table S4) and displayed the same phenotype for DnaQ foci number and stoichiometry within measurement error (Supplementary Figure S8).

For the transcriptional block perturbations, the *rpoB*35* mutant dual labelled strain exhibited no difference in the proportion of colocalised DnaQ or UvrD foci (Figure 3A and B). This mutant and all others tested exhibited the same predominant tetrameric stoichiometry trends as wild type (Supplementary Figure S12), with clear peaks at tetramer intervals in the colocalised stoichiometry distribution and less clear but still largely tetrameric intervals in the stoichiometry distribution for UvrD foci that are not colocalised with DnaQ. This provides further evidence that UvrD operates predominantly as a tetramer *in vivo*. We compared the mean stoichiometry for each mutant to that of wild type (Figure 3C and D). Unexpectedly, the *rpoB*35* mutant produced a slight but statistically significant increase in mean colocalised stoichiometry, corresponding to approximately one extra UvrD tetramer at the replication fork (Figure 3C). This finding may indicate the level of instability conferred by this mutation has multiple downstream effects that alter UvrD localisation significantly at the fork. Alternatively, it could mean that *rpoB*35* does not affect the

formation of the types of transcriptional block that are acted upon by UvrD. Rifampicin treatment produced a clearer response, reducing the number of DnaQ foci colocalised with UvrD by ~20% (Figure 3A) and the mean stoichiometry of colocalised and not colocalised UvrD foci by around one UvrD tetramer (Figure 3C and D). Single-molecule observations of RNAP have shown it to be significantly more mobile under rifampicin treatment (95), implying fewer RNAPs bound to DNA and fewer blocks to replication. Our rifampicin treatment results are consistent with fewer transcriptional blocks to replication reducing the amount of UvrD recruited to the replisome and support the hypothesis that UvrD is recruited by these replicative blocks.

By deleting *mutS* or *uvrA* we removed UvrD's role in mismatch repair and nucleotide excision repair respectively. Deleting *mutS* surprisingly resulted in no change in UvrD colocalisation with DnaQ but did increase the mean UvrD stoichiometry colocalised with DnaQ by around one tetramer (Figure 3A). In the Δ*uvrA* mutant this resulted in a clear drop of ~25% in UvrD colocalisation with DnaQ (Figure 3B) with no change in the number of UvrD foci (Supplementary Figure S8), consistent with the hypothesis that UvrD association with the fork is dependent on actively resolving DNA damage induced blocks to replication. The minimal response in the Δ*mutS* strain may also suggest that UvrD at the fork is more involved in nucleotide excision repair than mismatch repair.

UvrD has been shown to compensate for Rep in *rep* null mutants (12). We also tested what effect this mutation would have in our single-molecule assay. Surprisingly, *rep* deletion resulted in a steep drop in UvrD copy number (Supplementary Figure S10). The degree of colocalisation between UvrD and DnaQ remained unchanged compared to wild type (Figure 3A and B) but the stoichiometry of foci was reduced to a single UvrD tetramer (Figure 3C and D and Supplementary Figure 11), presumably due to the lower copy number and availability of UvrD. The drop in UvrD copy number may reflect complex regulatory shifts in response to losing such a key protein in Rep, although it is interesting that even at low copy numbers, a UvrD tetramer remains recruited to the fork. Double knockouts, deficient in both Rep and UvrD, are lethal (12) so this minimal helicase presence must be the limit required for survival.

The dynamic association of UvrD with the replication fork is dependent on repair processing

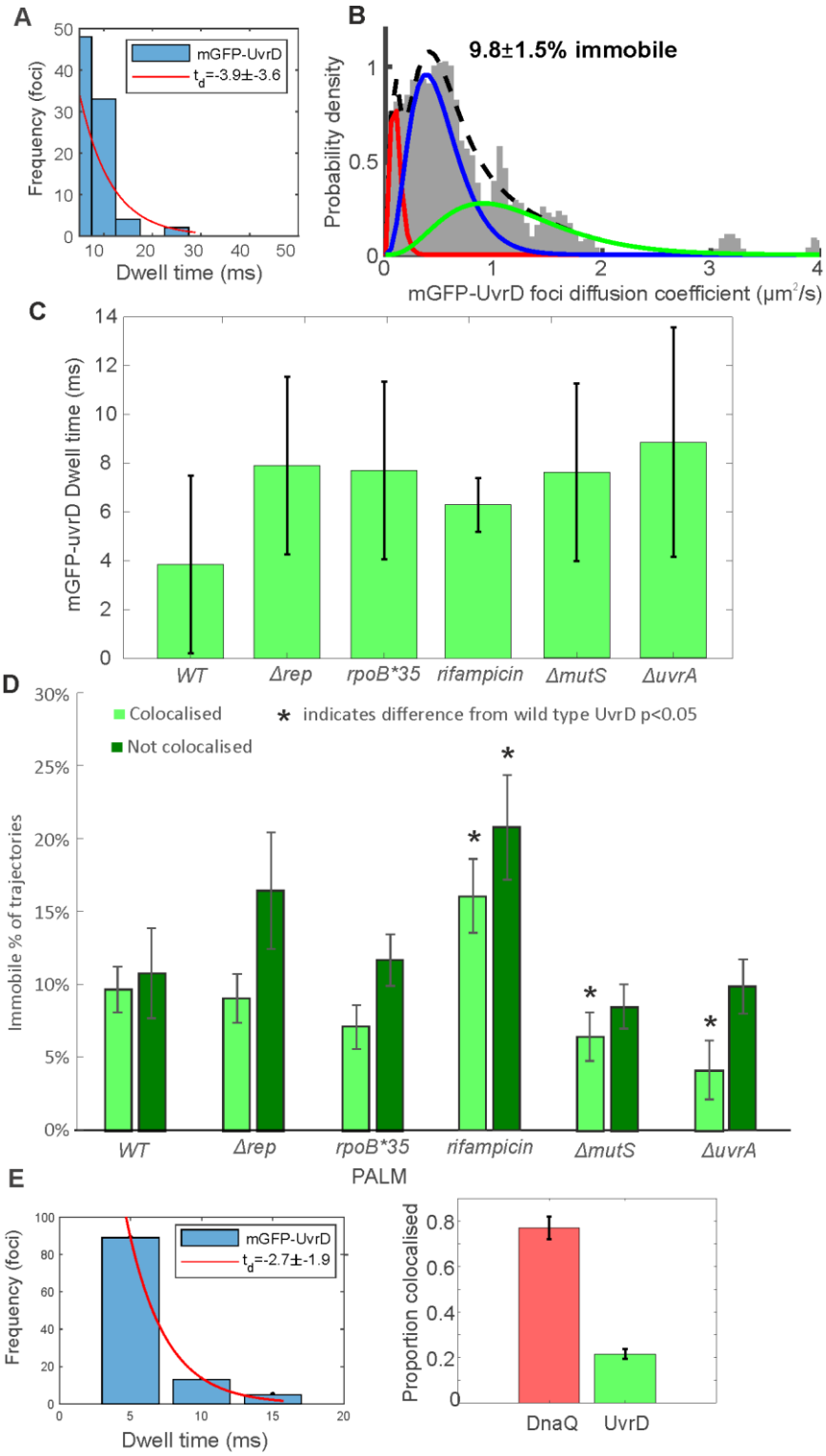

Figure 4: UvrD dynamics. A. Distribution of time over which UvrD and DnaQ foci were colocalised (blue) fitted with an exponential (red) to yield a characteristic dwell time. B. Distribution of microscopic diffusion coefficients of wild type UvrD foci (grey) fitted with a three state gamma distribution model containing a relatively immobile population with D = 0.1 μm^2/s (red), a transiently immobile population, D = 0.5 μm^2/s (blue) and a mobile population,

D=1.2 μm^2/s (green). C. The dwell times for each UvrD strain. Error bars represent the 95% confidence intervals on the fit. D. The proportion of UvrD foci in the immobile population for each UvrD strain colocalised or not colocalised with DnaQ foci location. Statistically significant differences $p<0.05$ from wild type indicated by *. E. PALM dwell time and colocalisation proportion of detected tracks.

By tracking UvrD foci as a function of time using rapid millisecond timescale sampling in Slimfield imaging, we were also able to characterize its dynamics in wild type and repair impaired cells. We measured the number of frames UvrD foci were colocalised with DnaQ foci positions, the dwell time, and calculated the apparent microscopic diffusion coefficient of individual foci (Figure 4 and Supplementary Figure S13). The UvrD dwell time at the fork for the wild type strain was measured to be approximately 4 ms, indicating a relatively dynamic association of UvrD at the replication fork. The apparent microscopic diffusion coefficients (*D*) were best fit with a three parameter Gamma model, containing a relatively immobile population with $D = 0.1$ μm^2/s, a transiently immobile population, $D = 0.5$ μm^2/s and a mobile population, D=1.2 μm^2/s, similar to Rep (13). In wild type, we found approximately 10% of UvrD foci were immobile, whether colocalised with the DnaQ fork location or not, with the rest of the foci split between the other two populations.

We sought to use these molecular measurements to determine the effect of perturbing UvrD-mediated DNA replication repair and block resolution on UvrD dynamics. All deletions resulted in a marginal though statistically negligible increase in dwell time to between 6-9 ms. The Δ*rep* and *rpoB*35* mutations resulted in no change in mobility from wild type. Rifampicin treatment however, resulted in an increase in the proportion of immobile foci both at and away from the fork. This finding appears counterintuitive as rifampicin treatment results in more mobile RNAP (95), however it is unclear what effect rifampicin has on the population of RNAP molecules that remain bound to DNA. These results may suggest that such blocks provide an increased barrier to replication, decreasing mobility of UvrD as it attempts to deal with these blocks. In the Δ*mutS* and Δ*uvrA* strains, the proportion of immobile foci decreased at the fork, again consistent with the hypothesis that UvrD association with the fork is dependent on DNA damage resolution activity. An alternative explanation for these results is that UvrD is less mobile when resolving DNA damage blocks to replication and more mobile when resolving transcriptional blocks, as reducing or

eliminating UvrD's role in these processes decreased or increased the immobile fraction in DNA repair and transcription impaired cells respectively (Figure 4).

In vitro experiments confirm block-dependent UvrD function

To further investigate the role of blocks in UvrD recruitment to the replisome, we performed a stalled replication assay *in vitro,* which allowed us to specifically vary the nucleoprotein block and the timing of UvrD recruitment i.e. before or after the replisome had encountered the block. *E. coli* replisomes can be reconstituted on plasmid DNA templates containing *oriC* and engineered stall sites. UvrD can be included from the start of replication or added after the replisome has encountered the nucleoprotein block. Blocked fork resolution was then probed by examining replication products by denaturing gel electrophoresis.

We first used an *oriC*-containing plasmid which contained a specific RNAP stall site ($P_{lacUV5\ 52C}$) to facilitate formation of a stalled transcription elongation complex via nucleotide deprivation. Stalled RNAP acts as a barrier to the replisome in both head-on and co-directional orientations and prevents the formation of full-length replication products (1). Arresting the replisome at this RNAP block resulted in replication products consisting of four truncated leading strands. The strand sizes matched those expected for replisomes moving clockwise or counter-clockwise from *oriC* and encountering $P_{lacUV5\ 52C}$ or the promoters within the *ColE1* plasmid origin of replication (Figure 5A, lane 2 and Figure 5C) (1).

Inclusion of UvrD before replication initiation enabled movement of replisomes through stalled RNAP and resulted in a decrease in all four truncated leading strand products and a concomitant increase in production of full-length leading strands (Figure 5A, lane 5 and 5E) (1). Addition of UvrD once the replisome had already encountered the block gave variable results that ranged from an inhibitory to a stronger effect, although differences were not statistically significant at $p<0.05$ (Figure 5A, compare lane 5 with 6, Figure 5E). Similar results were also obtained for Rep (Figure 5A, compare lane 3 with 4, Figure 5E). In the absence of replication neither Rep nor UvrD are capable of pushing stalled RNAP from the $P_{lacUV5\ 52C}$ stall site (1). We found that the mGFP tag does not prevent UvrD from dislodging a protein block (Supplementary Figure S14).

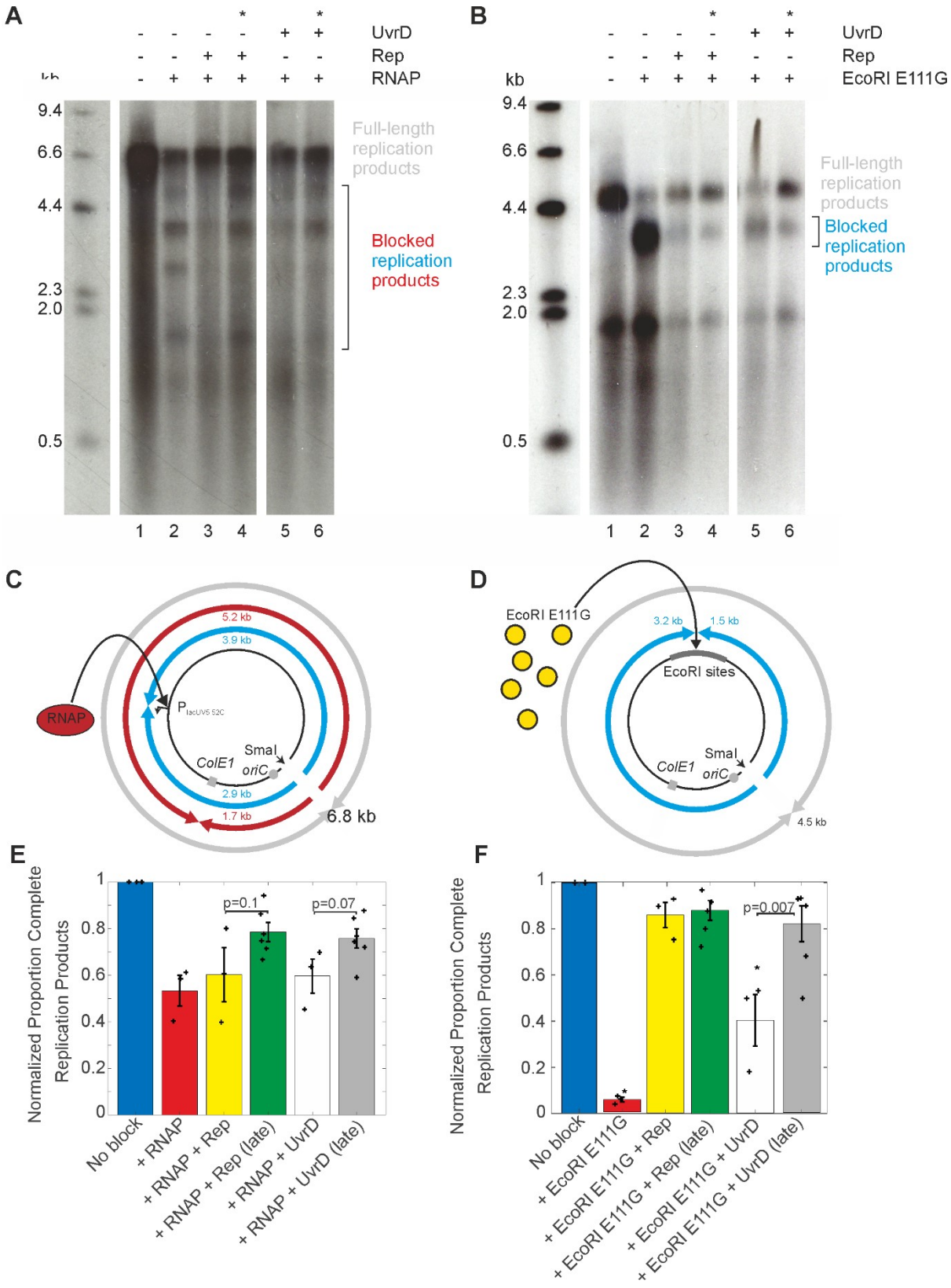

Figure 5: Helicase pre-association affects the promotion of replication fork movement through different nucleoprotein blocks A. Denaturing agarose gel of replication products formed from pPM872 (1) in the absence and presence of RNAP block, Rep and UvrD added pre- and post-collision (*) as indicated. B. Denaturing agarose gel of replication products formed from pPM594 (12) in the absence and presence of EcoRI E111G block, Rep and UvrD added pre- and post-collision (*) as indicated. Truncated leading strand products formed by

replisomes originating from *oriC* and colliding with RNAP (C) and EcoRI E111G (D). Quantification of lanes in (A) and (B) from three technical replicates shown in (E) and (F), with standard error in the mean indicated and each replicate result shown as a cross.

Since UvrD has been shown to interact with RNAP (47–49), we tested whether UvrD-block pre-association is a requirement for its promotion of replication. EcoRI E111G is a mutant restriction enzyme that binds to its recognition sequence but has reduced cleavage activity (96). EcoRI E111G can thus act as an engineered replication fork block that can be overcome by Rep or UvrD helicase activity (12). We tested whether UvrD helicase could promote replication through this barrier when added before or after initiation of replication on a plasmid template with an array of eight EcoRI sites (Figure 5B and D). Adding UvrD post-collision did not impede its promotion of replication; in fact the resolution of these collisions appeared to be more efficient because the proportion of full-length replication products increased (Figure 5B, compare lane 5 and 6, 5F). Quantification of full-length replication products as a proportion of reaction products showed that late UvrD addition increased full-length replication products to 84% (n=6) from 41% (n=3) when UvrD is present before fork collision. This contrasts with the RNAP block results where the UvrD-RNAP interaction (47–50) might be responsible for localising UvrD to the block and facilitating resolution, resulting in no difference when present pre- or post-collision. Similarly, Rep associates directly with the replication fork, also resulting in no difference when present pre- or post-collision, for both blocks. These results suggest that UvrD might recognize stalled replication forks at nucleoprotein blocks using a different mechanism than Rep. Combining these data with the lack of a specific replisome partner and reductions in colocalisation between UvrD and DnaQ fork marker when replication blocks are perturbed *in vivo*, leads us to propose that UvrD is present at the replication fork due to the high frequency of different types of blocks to replication.

DISCUSSION

Here, we show that the majority of replisomes are associated with UvrD; but unlike the established Rep association, UvrD has no interaction partner in the replisome. UvrD instead associates with the replisome through the frequent blocks to replication encountered by the fork. Similarly to Rep, *in vitro* evidence suggests UvrD functions poorly as a helicase when monomeric (97). We showed previously that functional Rep foci were hexameric *in vivo* but that this oligomerisation is due to interactions with

hexameric DnaB (13). Again, UvrD functions differently and appears to self-associate into tetramers, as evidenced here by tetramer periodicity at and away from the fork (Figure 2 and Supplementary Figure 11) and previous ultracentrifugation experiments *in vitro* (57). It is possible that UvrD may not have evolved to fulfil exactly the same function as Rep. It is common in many enzyme-catalysed reactions that if one enzyme is depleted then another will be available to take its place, but with a reduced catalytic efficiency (98). On initial inspection, this might appear to be the case for Rep and UvrD, in light of the lower efficiency of block resolution for UvrD compared to Rep, noting that deletion of Rep has a profound impact on replication whereas lack of UvrD does not (99). However, we have shown that Rep and UvrD have distinctly different modes of recruitment at a replication block. These differing mechanisms of replication promotion may suggest a model in which these accessory helicases have evolved to fulfil the same overall function (i.e. that of resolving a block to DNA replication) but in different ways. Even with different block removal efficiency, such redundancy may confer an increased level of robustness, helping to ensure that the vital process of DNA replication is carried out correctly by the cell.

We used single-molecule microscopy to show that a high proportion of forks, 80%, are associated with UvrD *in vivo.* Although the raw imaging data of our Slimfield microscopy is still subject to the optical resolution; the localization tracking algorithms applied can pinpoint fluorescently labelled UvrD to approximately 40 nm lateral precision, smaller than the 50 nm diameter of the replisome machinery itself (69) and equivalent to ~100 bp DNA. Thus, our measurements for colocalisation between UvrD and DnaQ are likely to be good indicators of a real interaction between the replication fork and UvrD. Importantly, the degree of colocalisation we observed is much higher than expectations of random overlap of the optical images of DnaQ-mCherry and mGFP-UvrD.

Through SPR, however, we could not find any interaction partner at the replisome apart from Tau. As a control, we tested Tau's interaction with a Rep helicase, and also found a positive interaction. Thus, we conclude that the interaction of UvrD with Tau is likely non-specific and UvrD recruitment to the replisome is mediated by blocks, rather than an interaction partner at the replisome. However, we cannot know the oligomeric state of UvrD on the SPR chip and UvrD's tetrameric form may affect its interactions with replisome components.

We probed UvrD's function at the replication fork by perturbing its known DNA repair processing functions, specifically by knocking out *mutS* and *uvrA*, thus blocking mismatch and nucleotide excision repair respectively. We also introduced a mutant RNAP with *rpoB*35* and treated the wild type with rifampicin to reduce the occurrence of transcriptional blocks to translocating replication machinery. Deleting *uvrA* and rifampicin treatment produced clear results, reduced fork colocalization, but deleting *mutS* and introducing the *rpoB*35* mutation did not. However these latter perturbations did result in an identical phenotype of one extra UvrD tetramer per fork. The *rpoB*35* mutation improves cell viability to increased DNA lesions (92). This intriguing link between mutations requires further study, possibly of these dual labelled strains in response to increased DNA lesions. These data support the hypothesis that UvrD is recruited to the replisome by replicative blocks. This is substantiated by the reduced frequency of colocalization observed when mismatch repair and nucleotide excision repair pathways involving UvrD are disrupted. RNA polymerases are the most frequently encountered barrier to replication and we also see a reduction in colocalization when RNA polymerases are removed by the antibiotic.

The only function of UvrD we did not probe directly here was its role in RecA-mediated recruitment. We believe the results from a *recA* knockdown would be difficult to interpret due to its pleiotropic effects. RecA is the principal recombinase and induces the complex SOS response resulting in the induction of UvrD expression (100, 101). Furthermore, UvrD removes RecA from RecA-DNA complexes, thus functioning as an antirecombinase (102–104). Dissecting these functions of UvrD from other effects that a *recA* mutation may have on the cell would be difficult. Applying the perturbations in combination, i.e. double knockdowns or knockdowns plus rifampicin, would likely lead to confusing results since too many deleterious perturbations may be lethal or change normal cell function too radically to be biologically relevant in the intended way.

For the suite of mutant strains investigated we found small but significant changes in colocalisation of UvrD with the replication fork, implying that UvrD is recruited to the replication fork by the frequent blocks to replication it encounters. For example, the UvrD-RNAP interaction could localise UvrD to the vicinity of active transcription machinery (50). Since RNA polymerase is the most common replication block, a secondary consequence would be UvrD-fork colocalisation. This is in contrast to the Rep accessory helicase which has a specific interaction partner in the replisome

of the replicative helicase DnaB (89). Recent biochemical findings *in vitro* show that blocks to replication occur very frequently (1)(19)(105), potentially accounting for our finding that UvrD colocalises with the fork more frequently than Rep, despite Rep having a specific interaction partner at the fork.

We have shown that replication forks stalled at transcriptional blocks can be rescued by addition of UvrD, prior to or post-stalling. If UvrD is to help perform this function then it must be present during the resolution of collision between the replication and transcription machinery, however, our estimate for dwell time at the fork of just a few milliseconds (compared to seconds for DnaQ (79)) suggests a non-negligible dissociation constant; UvrD is not processive *per se* but rather undergoes rapid turnover at the fork such that there is a high likelihood for UvrD being present at any given time, but not necessarily the same set of molecules. Interestingly we observed a similar dwell time for Rep (13), despite it having a clear association partner in DnaB at the fork. However, using a defective restriction enzyme EcoRI E111G block produced a different effect, with late UvrD addition improving block resolution. This restriction enzyme block is artificial and less biologically relevant but may indicate that the known specific UvrD interaction with RNAP is important. Improved replication resolution with late addition of UvrD is intriguing, implying increased affinity for or activity at pre-stalled replication forks compared to UvrD being present as the fork stalls. Complete understanding requires further study of replication block resolution in different conditions.

Our results suggest a model where UvrD diffuses and transiently interacts with DNA at random or through specific interactions such as with RNAP or a specific conformation of the blocked replication fork. At the DNA, UvrD is predominantly tetrameric, either pre-assembling in solution or on the DNA itself. The frequent sampling leads to UvrD often being in the vicinity of the replisome, allowing UvrD to resolve the frequent blocks to replication. It is also possible that certain barriers to replication may be harder for Rep to resolve, and such barriers can possibly be more efficiently removed by UvrD, however, it is still likely to be the case that they do not directly challenge the ability of the cell to replicate the genome in light of *uvrD* deletion still resulting in viable cells. Indeed, UvrD shares a high degree of structural similarity with Rep, although the two proteins differ significantly in their amino acid sequences (31, 106). While Rep is recruited to the fork through specific interactions with DnaB,

no such interaction could be identified for UvrD. Stochastic impairment of the ability of Rep to interact with DnaB may necessitate block processing at the fork by UvrD. In summary, our results highlight the contribution of UvrD action to facilitating accurate genome duplication at active replisomes.

MATERIALS AND METHODS

Strain construction

All strains used in this study (listed in full in SI Table S1, with associated plasmids and primers in SI Tables S2 and S3) are derivatives of the laboratory wild type strain TB28. Tagging of *dnaQ-mCherry-<kan>* (C-terminally labelled) is described in (13). *mGFP-uvrD-<kan>* (N-terminally labelled) was amplified from plasmid pAS79 (*uvrD*$^{+}$) with primers oAS145 and oJGB383 having 50 bp homology to either end of the native *uvrD* locus. The resulting PCR product had homology either side such that recombination with the chromosome would result in integration of the PCR product at the native locus under the control of the native promoter. Prior to integration, all PCR products were treated with DpnI, gel purified, and introduced by electroporation into cells expressing the lambda Red genes from the plasmid pKD46 (55). The recombinants were selected for kanamycin resistance and screened for ampicillin sensitivity. The colonies obtained were verified for integration by PCR and sequencing. The *uvrD* recombinants were verified by PCR amplification using primers oPM319 and oPM320, and sequencing using the primers oJGB417, oJGB418, oPM407, oPM409, oPM411, and oMKG71. Where required, the kanamycin resistance gene was removed by expressing Flp recombinase from the plasmid pCP20 (58) to generate kanamycin sensitive strains carrying the fluorescent protein (FP) fusions. Dual labelled strains were created by introducing the kanamycin tagged FP alleles by standard P1 mediated transduction into single labelled strains carrying the required FP allele after removing the linked kanamycin marker.

Determination of cell doubling time

E. coli strains were grown overnight in LB medium at 37°C at 200 rpm shaking. The saturated overnight cultures were diluted 100 fold into fresh LB or washed once with 1X 56 salts and diluted 100 fold in fresh 1X 56 salts with 0.2% glucose as the carbon source. Aliquots of 100 µl each of the diluted cultures in fresh media were pipetted

518 into individual wells of 96 well clear flat bottom sterile microplates (Corning). The
519 microplates containing the diluted cultures were incubated in a BMG LABTECH
520 SPECTROstar Nano microplate reader at 37°C and the optical density (A_{600}) values
521 were recorded at defined time intervals. The time taken for the optical density values
522 to increase two fold during the exponential growth phase of the culture was taken as
523 the cell doubling time (SI Table S4, Supplementary Figure S1).

524 **Protein Overexpression and Purification**

525 *mGFP-uvrD* was excised from pAS79 using XhoI and SalI and ligated into pET14b
526 cut with XhoI, creating pAS152 encoding N-terminal histidine-tagged mGFP-UvrD.
527 pAS152 was used to overexpress the mGFP-UvrD fusion in Rosetta™
528 2(DE3)/pLysS. The cells were grown in LB medium containing 100 µg/ml ampicillin
529 and 30 µg/ml chloramphenicol at 37ºC and 220 rpm to OD_{600} ~ 0.7. The cultures
530 were then equilibrated to room temperature and overexpression was induced by
531 adding 1 mM IPTG and incubating at 16ºC for 24 hours. Cells from the expressed
532 culture were collected by centrifugation at 4ºC and frozen at -80ºC. The cells were
533 later thawed on ice and resuspended in buffer A (20 mM Tris-Cl pH 8.3, 500 mM
534 NaCl, 5 mM imidazole, 10% glycerol) along with 0.1 mg/ml lysozyme, 1 mM AEBSF,
535 0.7 µg/ml pepstatin, 0.5 µg/ml leupeptin, 2.5 µg/ml DNase I and 20 µg/ml RNase A
536 and incubated on ice for 30 minutes. Brij-58 was then added to a final concentration
537 of 0.1% v/v and incubated on ice for another 20 minutes. The suspension was
538 sonicated and then clarified by centrifugation at 18,000 rpm for 60 minutes at 4ºC in
539 an SS-34 rotor to remove debris. The lysate containing mGFP-UvrD was applied to a
540 5 ml His-trap FF crude column (GE healthcare) and the protein was purified by
541 chromatography on an imidazole gradient in buffer A. Peak fractions were collected
542 and concentrated using a Vivaspin 500 concentrator (30 kDa MWCO) (Sartorius).
543 Samples were then aliquoted and flash frozen in liquid nitrogen before storage at -
544 80ºC. Protein concentration was determined by Bradford's assay.

545 UvrD was purified as previously described (59). Briefly UvrD was overexpressed in
546 BL21-AI from a pETDuet vector, via induction by IPTG and arabinose. UvrD was
547 purified from the soluble cell extract after lysis through the use of affinity (heparin
548 agarose), anion exchange (Q-sepharose), and gel filtration chromatography. Pure
549 UvrD was then stored at -80ºC after dialysis into storage buffer or used immediately

550 in Size Exclusion Chromatography - Multi-Angle Laser Light Scattering (SEC-
551 MALLS) analysis.

552 Biotinylated UvrD and Rep were purified as previously described (60). Briefly, the
553 proteins were overexpressed in a BL21 (DE3) containing pBirAcm, encoding a biotin
554 ligase via induction by IPTG and the addition of biotin to the growth media. The
555 biotinylated proteins were then purified from the soluble cell extracts by ammonium
556 sulphate precipitation, and affinity chromatography (softlink avidin and heparin
557 agarose). Pure proteins were then dialysed into storage buffer overnight and stored
558 at -80°C

559 **Helicase assay**

560 Assays for unwinding of streptavidin-bound forks were performed using a substrate
561 made by annealing oligonucleotides oPM187B20 (5' end labelled with ^{32}P) and
562 oPM188B34. Reactions were performed in 10 µL volumes containing 40 mM HEPES
563 (pH 8); 10 mM DTT; 10 mM magnesium acetate; 2 mM ATP; 0.1 mg ml^{-1} BSA and
564 1 nM forked DNA substrate. Reactions were carried out as described earlier (13, 61).
565 Briefly, the reaction mixture was pre-incubated at 37°C for five minutes with or
566 without 1 µM streptavidin (Sigma-Aldrich), to which helicase (as indicated) and biotin
567 (Sigma-Aldrich) were added to 100 µM (acting as a trap for free streptavidin) and
568 incubated at 37°C for another 10 minutes. Reactions were stopped by addition of 2.5
569 µl of 2.5% SDS, 200 mM EDTA and 10 mg ml^{-1} of proteinase K. Reactions were then
570 analysed by non-denaturing gel electrophoresis on 10% polyacrylamide TBE gels.
571 The quantification of the unwinding and displacement of streptavidin from the fork
572 was carried out as described in (62).

573 **Preparation of cells for microscopy**

574 Cells were grown overnight in LB to saturation. The overnight cultures were
575 inoculated the next day at 1:1000 dilution in 1X 56 salts supplemented with 0.2%
576 glucose as the carbon source. The dilutions were then grown at 30°C to mid-log
577 phase.

578 **Rifampicin treatment**

Cells prepared for microscopy were treated with rifampicin at a final concentration of 50 μg/mL for 30 minutes at 30°C.

Microscopy and image analysis

Imaging was performed on a bespoke dual-colour single-molecule microscope (13). Excitation from Obis 488 nm and 561 nm wavelength 50mW lasers (run at 20 mW) was reduced to 10 μm at full width half maximum field in the sample plane producing Slimfield illumination (63) producing a mean excitation intensity of ~0.25 mW/μm^2. Lasers were digitally modulated to 5 ms period to produce alternating laser excitation using National Instruments dynamic I/O module NI 9402. Excitation was coupled into a Zeiss microscope body with the sample mounted on a Mad City Labs nanostage. Images were magnified to 80nm/pixel and imaged using an Andor Ixon 128 emCCD camera. Colour channels were split red/green using a bespoke colour splitter consisting of a dual-pass green/red dichroic mirror centred at long-pass wavelength 560 nm and emission filters with 25 nm bandwidths centred at 542 nm and 594 nm.

Cells were imaged on agarose pads suffused with minimal media as described previously (64). Foci were detected and tracked using previously described bespoke MATLAB software (65). In brief, bright candidate foci were detected in each frame by image transformation and thresholding. A 17x17 pixel region of interest (ROI) is drawn around each candidate and subjected to iterative Gaussian masking (66). Foci were accepted if their signal to noise ratio was above 0.4. Foci in successive frames were linked together into trajectories based on nearest distance, provided it was < 5 pixels. Linked foci were accepted as “tracks” nominally if they persist for at least 4 consecutive image frames.

Characteristic intensity of mGFP or mCherry was determined from the distribution of foci intensity values towards the end of the photobleach confirmed by overtracking foci beyond their bleaching and applying an edge-preserving filter (67, 68) to the raw intensity data to generate individual steps of the characteristic intensity, due to photobleaching (Supplementary Figure S7). This intensity was used to determine the stoichiometry of foci by fitting the first 3 intensity points with a straight line and dividing the intercept by this characteristic intensity. The number of peaks in the Gaussian fits to UvrD was set by running a peak fitting algorithm over the wild type distribution. This number of Gaussians was then used for mutant distributions unless

two or more of the Gaussians converged on the same/similar peak value, in which case they were removed. For DnaQ, two peaks were fit as used previously (69).

GFP and mCherry images were aligned based on the peak of the 2D cross correlation between their respective brightfield images. Colocalisation between foci and the probability of random colocalisation was determined as described previously (70, 71).

The microscopic apparent diffusion coefficients (*D*) were determined by fitting a straight line to the first three mean squared displacements (MSD) values constrained through the equivalent localization precision MSD as determined from the intensity (72, 73). *D* distributions were fit by three Gamma distributions as described previously (74–76). Dwell time was calculated as the number of frames that each trajectory was colocalised with the fork position, as determined by the DnaQ foci detected at time zero.

SEC-MALLS

Size Exclusion Chromatography – Multi-Angle Laser Light Scattering (SEC-MALLS) experiments used Wyatt HELEOS-II multi-angle light scattering and rEX refractive index detectors linked to a Shimadzu HPLC system (SPD-20A UV detector, LC20-AD isocratic pump system, DGU-20A3 degasser and SIL-20A autosampler) with a G.E. Superdex S200 10/300 column at a flow rate of 0.5 mL/min in buffer of 20 mM Tris pH 8.3 (at 4degC) 1 mM EDTA, 1 mm EGTA, 1 mM DTT, 200 mM NaCl, 5% glycerol buffer. Data were analysed using Wyatt Astra 7 software. MWs were estimated using the Zimm fit method with degree 1. A value of 0.182 mL/g was used for protein refractive index increment (dn/dc).

Surface plasmon resonance (SPR)

SPR was performed at 25°C on a BIAcore T200 instrument as in (12). Immobilisation of *E. coli* UvrD and Rep was performed onto streptavidin-coated SA sensor chips whilst the indicated concentrations of Tau and UvrB were passed over in 10 mM HEPES pH 7.4, 3 mM EDTA, 150 mM NaCl, 10 mM $MgCl_2$ and 0.005% Tween 20 at 20 µl min^{-1}. This buffer differed from that used in the DNA replication assays to minimise non-specific interactions with the surface-immobilised streptavidin.

Replication assay

Replication assays were carried out using pPM872 as the template for RNAP blocks (1) or pPM594 (12) for EcoRI E111G blocks. Plasmid pPM872 contains $P_{lacUV5\ 52C}$, a strong promoter in which the first 52 nucleotides of the transcript lack cytosine residues and are then followed by four consecutive cytosines. This enables transcription of $P_{lacUV5\ 52C}$ to be stalled by the omission of CTP. Assays were performed in 40 mM HEPES (pH 8); 10 mM DTT; 10 mM magnesium acetate; 2 mM ATP; 0.2 mM GTP, 0.2 mM UTP; 0.04 mM dNTPs; and 0.1 mg/ml BSA. Reactions (15 µl) contained 2 nM plasmid template, 50 nM DNA polymerase III αεθ complex, 25 nM τ clamp loader complex, 160 nM DnaB and DnaC monomers, 1 µM SSB, 80 nM β clamp, 30 nM HU, 200 nM DnaG, 300 nM DnaA. Helicases were added as indicated. Rep and UvrD used at 200 nM. *E. coli* RNAP holoenzyme from NEB (1 U/µl) was used at 1/3 dilution. Dilution was determined empirically to match RNAP replication inhibition levels from (1). EcoRI E111G was purified as in (77) and used at 200 nM. Reactions were assembled on ice and initiated by addition of DnaA and incubation for 4 min at 37°C, followed by addition of 60 units SmaI (Promega) plus 0.4 MBq [α^{32}P] dCTP (222 TBq/mmol). Standard reactions with the helicase present in the initial protein mix were carried out at 37°C for 1 minute and then terminated by addition of 1 µl of 0.5 M EDTA. Delayed helicase addition was carried out by adding Rep/UvrD after 1 minute and incubation for a further minute at 37°C before termination with EDTA. Ethanol precipitated replication products were analysed by denaturing agarose gel electrophoresis (0.7% agarose in 2 mM EDTA, 30 mM NaOH for 400 volt hours, standard run was 16 hours at 25 V), phosphorimaging and autoradiography. 5'-labelled HindIII- digested lambda DNA was used as a marker. Gels were quantified using Quantity One® (Bio-Rad) software. Full-length plasmid replication products were quantified as a proportion of summed blocked products and normalised for length (for EcoRI E111G block), or total lane signal (RNAP block).

Acknowledgments

We thank Maria Chechik for help with mGFP-UvrD purification. We thank Prof. Nigel Savery (University of Bristol) for the gift of the pETDuet-UvrD overexpression plasmid.

673 We thank the Molecular Interactions Laboratory in the Bioscience Technology Facility
674 at the University of York for technical assistance and support.

675

676 **Funding**

677 Supported by BBSRC via grants BB/N006453/1 (M.L., P.M.), BB/R001235/1 (M.L.,
678 (M.L.,P.M.,A.S.), BB/N014863/1 (M.H.).

679
680

681

682

REFERENCES

1. M. Hawkins, *et al.*, Direct removal of RNA polymerase barriers to replication by accessory replicative helicases. *Nucleic Acids Res.* **47** (2019).
2. R. T. Pomerantz, M. O'Donnell, The replisome uses mRNA as a primer after colliding with RNA polymerase. *Nature* **456**, 762–767 (2008).
3. H. Merrikh, C. Machón, W. H. Grainger, A. D. Grossman, P. Soultanas, Co-directional replication-transcription conflicts lead to replication restart. *Nature* **470**, 554–7 (2011).
4. A. H. Syeda, J. Atkinson, R. G. Lloyd, P. McGlynn, The balance between recombination enzymes and accessory replicative helicases in facilitating genome duplication. *Genes (Basel).* **7** (2016).
5. A. Helmrich, M. Ballarino, L. Tora, Collisions between replication and transcription complexes cause common fragile site instability at the longest human genes. *Mol. Cell* **44**, 966–977 (2011).
6. Y. Takeuchi, T. Horiuchi, T. Kobayashi, Transcription-dependent recombination and the role of fork collision in yeast rDNA. *Genes Dev.* **17**, 1497–1506 (2003).
7. A. L. de Septenville, S. Duigou, H. Boubakri, B. Michel, Replication fork reversal after replication-transcription collision. *PLoS Genet.* **8** (2012).
8. C. J. Rudolph, A. L. Upton, A. Stockum, C. A. Nieduszynski, R. G. Lloyd, Avoiding chromosome pathology when replication forks collide. *Nature* **500**, 608–611 (2013).
9. B. Michel, G. Grompone, M. J. Florès, V. Bidnenko, Multiple pathways process stalled replication forks. *Proc. Natl. Acad. Sci. U. S. A.* **101**, 12783–12788 (2004).
10. E. V. Mirkin, S. M. Mirkin, Mechanisms of transcription-replication collisions in bacteria. *Mol. Cell. Biol.* **25**, 888–895 (2005).
11. P. McGlynn, N. J. Savery, M. S. Dillingham, The conflict between DNA replication and transcription. *Mol. Microbiol.* **85**, 12–20 (2012).
12. C. P. Guy, *et al.*, Rep provides a second motor at the replisome to promote duplication of protein-bound DNA. *Mol. Cell* **36**, 654–666 (2009).
13. A. H. Syeda, *et al.*, Single-molecule live cell imaging of Rep reveals the dynamic interplay between an accessory replicative helicase and the replisome. *Nucleic Acids Res.* **47**, 6287–6298 (2019).
14. P. McGlynn, Linking transcription with DNA repair, damage tolerance, and genome duplication. *Proc. Natl. Acad. Sci. U. S. A.* **107**, 15314–15315 (2010).
15. D. Dutta, K. Shatalin, V. Epshtein, M. E. Gottesman, E. Nudler, Linking RNA polymerase backtracking to genome instability in E. coli. *Cell* **146**, 533–543 (2011).
16. D. Duchi, *et al.*, RNA Polymerase Pausing during Initial Transcription. *Mol. Cell* **63**, 939–950 (2016).
17. G. Ghosal, J. Chen, DNA damage tolerance: a double-edged sword guarding the genome. *Transl. Cancer Res.* **2**, 107–129 (2013).
18. S. Hamperl, M. J. Bocek, J. C. Saldivar, T. Swigut, K. A. Cimprich, Transcription-Replication Conflict Orientation Modulates R-Loop Levels and Activates Distinct DNA Damage Responses. *Cell* **170**, 774-786.e19 (2017).
19. K. Hizume, H. Araki, Replication fork pausing at protein barriers on chromosomes. *FEBS Lett.* **593**, 1449–1458 (2019).
20. K. K. Myka, M. E. Gottesman, DksA and DNA double-strand break repair.

Curr. Genet. **65**, 1297–1300 (2019).
21. K. K. Myka, *et al.*, Inhibiting translation elongation can aid genome duplication in Escherichia coli. *Nucleic Acids Res.* **45**, 2571–2584 (2017).
22. S. M. Mangiameli, C. N. Merrikh, P. A. Wiggins, H. Merrikh, Transcription leads to pervasive replisome instability in bacteria. *Elife* **6** (2017).
23. V. Kamarthapu, *et al.*, ppGpp couples transcription to DNA repair in E. coli. *Science* **352**, 993–996 (2016).
24. B. J. Brewer, When polymerases collide: replication and the transcriptional organization of the E. coli chromosome. *Cell* **53**, 679–686 (1988).
25. A. Srivatsan, A. Tehranchi, D. M. MacAlpine, J. D. Wang, Co-orientation of replication and transcription preserves genome integrity. *PLoS Genet.* **6** (2010).
26. B. Liu, B. M. Alberts, Head-on collision between a DNA replication apparatus and RNA polymerase transcription complex. *Science* **267**, 1131–1137 (1995).
27. J. D. Wang, M. B. Berkmen, A. D. Grossman, Genome-wide coorientation of replication and transcription reduces adverse effects on replication in Bacillus subtilis. *Proc. Natl. Acad. Sci. U. S. A.* **104**, 5608–5613 (2007).
28. T. S. Sankar, B. D. Wastuwidyaningtyas, Y. Dong, S. A. Lewis, J. D. Wang, The nature of mutations induced by replication–transcription collisions. *Nature* **535**, 178–181 (2016).
29. D. Ivanova, *et al.*, Shaping the landscape of the Escherichia coli chromosome: replication-transcription encounters in cells with an ectopic replication origin. *Nucleic Acids Res.* **43**, 7865–7877 (2015).
30. A. Helmrich, M. Ballarino, E. Nudler, L. Tora, Transcription-replication encounters, consequences and genomic instability. *Nat. Struct. Mol. Biol.* **20**, 412–418 (2013).
31. J. G. Brüning, J. L. Howard, P. McGlynn, Accessory replicative helicases and the replication of protein-bound DNA. *J. Mol. Biol.* **426**, 3917–3928 (2014).
32. K. R. McDonald, *et al.*, Pfh1 Is an Accessory Replicative Helicase that Interacts with the Replisome to Facilitate Fork Progression and Preserve Genome Integrity. *PLoS Genet.* **12** (2016).
33. J. E. Sokoloski, A. G. Kozlov, R. Galletto, T. M. Lohman, Chemo-mechanical pushing of proteins along single-stranded DNA. *Proc. Natl. Acad. Sci. U. S. A.* **113**, 6194–6199 (2016).
34. G. D. Schauer, *et al.*, Replisome bypass of a protein-based R-loop block by Pif1. *Proc. Natl. Acad. Sci. U. S. A.* **117**, 30354–30361 (2020).
35. M. K. Gupta, *et al.*, Protein-DNA complexes are the primary sources of replication fork pausing in Escherichia coli. *Proc. Natl. Acad. Sci. U. S. A.* **110**, 7252–7257 (2013).
36. H. Boubakri, A. L. De Septenville, E. Viguera, B. Michel, The helicases DinG, Rep and UvrD cooperate to promote replication across transcription units in vivo. *EMBO J.* **29**, 145–157 (2010).
37. X. Liu, J. X. Seet, Y. Shi, P. R. Bianco, Rep and UvrD Antagonize One Another at Stalled Replication Forks and This Is Exacerbated by SSB. *ACS Omega* **4**, 5180–5196 (2019).
38. O. Adebali, Y. Y. Chiou, J. Hu, A. Sancar, C. P. Selby, Genome-wide transcription-coupled repair in Escherichia coli is mediated by the Mfd translocase. *Proc. Natl. Acad. Sci. U. S. A.* **114**, E2116–E2125 (2017).
39. N. Kang, E. Choi, S. G. Kim, J. Hwang, Inhibitory effect of UvrD and DinG on the replication of ColE1-derived plasmids in Escherichia coli. *Plasmid* **81**, 32–

41 (2015).
40. V. Epshtein, UvrD helicase: an old dog with a new trick: how one step backward leads to many steps forward. *Bioessays* **37**, 12–19 (2015).
41. P. R. Caron, S. R. Kushner, L. Grossman, Involvement of helicase II (uvrD gene product) and DNA polymerase I in excision mediated by the uvrABC protein complex. *Proc. Natl. Acad. Sci. U. S. A.* **82**, 4925–4929 (1985).
42. B. Van Houten. Nucleotide excision repair in Escherichia coli. *Microbiol. Rev.* **54**, 18–51 (1990).
43. A. L. Lu, S. Clark, P. Modrich, Methyl-directed repair of DNA base-pair mismatches in vitro. *Proc. Natl. Acad. Sci. U. S. A.* **80**, 4639–4643 (1983).
44. S. W. Matson, A. B. Robertson, The UvrD helicase and its modulation by the mismatch repair protein MutL. *Nucleic Acids Res.* **34**, 4089–4097 (2006).
45. L. Manelyte, *et al.*, The unstructured C-terminal extension of UvrD interacts with UvrB, but is dispensable for nucleotide excision repair. *DNA Repair (Amst).* **8**, 1300–1310 (2009).
46. A. B. Robertson, S. R. Pattishall, E. A. Gibbons, S. W. Matson, MutL-catalyzed ATP hydrolysis is required at a post-UvrD loading step in methyl-directed mismatch repair. *J. Biol. Chem.* **281**, 19949–19959 (2006).
47. E. J. Gwynn, *et al.*, The conserved C-terminus of the PcrA/UvrD helicase interacts directly with RNA polymerase. *PLoS One* **8** (2013).
48. K. Sanders, *et al.*, The structure and function of an RNA polymerase interaction domain in the PcrA/UvrD helicase. *Nucleic Acids Res.* **45**, 3875–3887 (2017).
49. V. Epshtein, *et al.*, UvrD facilitates DNA repair by pulling RNA polymerase backwards. *Nature* **505**, 372–377 (2014).
50. B. K. Bharati, *et al.*, Crucial role and mechanism of transcription-coupled DNA repair in bacteria. *Nature* **604**, 152–159 (2022).
51. B. Martinez, B. K. Bharati, V. Epshtein, E. Nudler, Pervasive Transcription-coupled DNA repair in E. coli. *Nat. Commun.* **13** (2022).
52. N. M. Haines, Y. I. T. Kim, A. J. Smith, N. J. Savery, Stalled transcription complexes promote DNA repair at a distance. *Proc. Natl. Acad. Sci. U. S. A.* **111**, 4037–4042 (2014).
53. A. J. Smith, N. J. Savery, Effects of the bacterial transcription-repair coupling factor during transcription of DNA containing non-bulky lesions. *DNA Repair (Amst).* **7**, 1670–1679 (2008).
54. A. J. Smith, N. J. Savery, RNA polymerase mutants defective in the initiation of transcription-coupled DNA repair. *Nucleic Acids Res.* **33**, 755–764 (2005).
55. J. Atkinson, *et al.*, Stimulation of UvrD helicase by UvrAB. *J. Biol. Chem.* **284**, 9612–9623 (2009).
56. R. P. Wong, N. García-Rodríguez, N. Zilio, M. Hanulová, H. D. Ulrich, Processing of DNA Polymerase-Blocking Lesions during Genome Replication Is Spatially and Temporally Segregated from Replication Forks. *Mol. Cell* **77**, 3-16.e4 (2020).
57. N. K. Maluf, T. M. Lohman, Self-association equilibria of Escherichia coli UvrD helicase studied by analytical ultracentrifugation. *J. Mol. Biol.* **325**, 889–912 (2003).
58. K. A. Datsenko, B. L. Wanner, One-step inactivation of chromosomal genes in Escherichia coli K-12 using PCR products. *Proc. Natl. Acad. Sci. U. S. A.* **97**, 6640–6645 (2000).
59. J. Atkinson, *et al.*, Stimulation of UvrD helicase by UvrAB. *J. Biol. Chem.* **284**,

9612–9623 (2009).
60. C. P. Guy, *et al.*, Rep provides a second motor at the replisome to promote duplication of protein-bound DNA. *Mol. Cell* **36**, 654–666 (2009).
61. J. G. Brüning, J. A. L. Howard, K. K. Myka, M. S. Dillingham, P. McGlynn, The 2B subdomain of Rep helicase links translocation along DNA with protein displacement. *Nucleic Acids Res.* **46**, 8917–8925 (2018).
62. J. G. Brüning, J. A. L. Howard, P. McGlynn, Use of streptavidin bound to biotinylated DNA structures as model substrates for analysis of nucleoprotein complex disruption by helicases. *Methods* **108**, 48–55 (2016).
63. M. Plank, G. H. Wadhams, M. C. Leake, Millisecond timescale slimfield imaging and automated quantification of single fluorescent protein molecules for use in probing complex biological processes. *Integr. Biol.* **1**, 602–612 (2009).
64. A. J. M. Wollman, A. H. Syeda, P. McGlynn, M. C. Leake, Single-Molecule Observation of DNA Replication Repair Pathways in E. coli. *Adv. Exp. Med. Biol.* **915**, 5–16 (2016).
65. H. Miller, *et al.*, Superresolution imaging of single DNA molecules using stochastic photoblinking of minor groove and intercalating dyes. *Methods* **88**, 81–8 (2015).
66. M. C. Leake, *et al.*, Stoichiometry and turnover in single, functioning membrane protein complexes. *Nature* **443**, 355–358 (2006).
67. M. C. Leake, D. Wilson, B. Bullard, R. M. Simmons, The elasticity of single kettin molecules using a two-bead laser-tweezers assay. *FEBS Lett.* **535**, 55–60 (2003).
68. M. C. Leake, D. Wilson, M. Gautel, R. M. Simmons, The elasticity of single titin molecules using a two-bead optical tweezers assay. *Biophys. J.* **87**, 1112–35 (2004).
69. R. Reyes-Lamothe, D. J. Sherratt, M. C. Leake, Stoichiometry and architecture of active DNA replication machinery in Escherichia coli. *Science* **328**, 498–501 (2010).
70. I. Llorente-Garcia, *et al.*, Single-molecule in vivo imaging of bacterial respiratory complexes indicates delocalized oxidative phosphorylation. *Biochim. Biophys. Acta* **1837**, 811–24 (2014).
71. A. J. M. Wollman, *et al.*, Critical roles for EGFR and EGFR-HER2 clusters in EGF binding of SW620 human carcinoma cells. *J. R. Soc. Interface* **19** (2022).
72. A. J. M. Wollman, M. C. Leake, Millisecond single-molecule localization microscopy combined with convolution analysis and automated image segmentation to determine protein concentrations in complexly structured, functional cells, one cell at a time. *Faraday Discuss.* **184**, 401–24 (2015).
73. M. C. Leake, *et al.*, Variable stoichiometry of the TatA component of the twin-arginine protein transport system observed by in vivo single-molecule imaging. *Proc. Natl. Acad. Sci. U. S. A.* **105**, 15376–81 (2008).
74. H. Miller, *et al.*, High-Speed Single-Molecule Tracking of CXCL13 in the B-Follicle. *Front. Immunol.* **9**, 1073 (2018).
75. J. Cosgrove, *et al.*, B cell zone reticular cell microenvironments shape CXCL13 gradient formation. *Nat. Commun.* **11** (2020).
76. X. Jin, *et al.*, Membraneless organelles formed by liquid-liquid phase separation increase bacterial fitness. *Sci. Adv.* **7** (2021).
77. S.-C. Chengs, R. Kim, K. Kings, S.-H. Kim, P. Modrich, Isolation of Gram Quantities of EcoRI Restriction and Modification Enzymes from an

Overproducing Strain. *J. Biol. Chem.* **259**, 11571–11575 (1984).
78. A. Badrinarayanan, R. Reyes-Lamothe, S. Uphoff, M. C. Leake, D. J. Sherratt, In vivo architecture and action of bacterial structural maintenance of chromosome proteins. *Science* **338**, 528–31 (2012).
79. T. R. Beattie, *et al.*, Frequent exchange of the DNA polymerase during bacterial chromosome replication. *Elife* **6**, e21763 (2017).
80. R. Reyes-Lamothe, C. Possoz, O. Danilova, D. J. Sherratt, Independent positioning and action of Escherichia coli replisomes in live cells. *Cell* **133**, 90–102 (2008).
81. A. L. Payne-Dwyer, A. H. Syeda, J. W. Shepherd, L. Frame, M. C. Leake, RecA and RecB: probing complexes of DNA repair proteins with mitomycin C in live Escherichia coli with single-molecule sensitivity. *bioRxiv*, 2021.10.04.463068 (2021).
82. D. A. Zacharias, J. D. Violin, A. C. Newton, R. Y. Tsien, Partitioning of lipid-modified monomeric GFPs into membrane microdomains of live cells. *Science* **296**, 913–916 (2002).
83. N. K. Maluf, C. J. Fischer, T. M. Lohman, A Dimer of Escherichia coli UvrD is the active form of the helicase in vitro. *J. Mol. Biol.* **325**, 913–935 (2003).
84. H. Yokota, Y. A. Chujo, Y. Harada, Single-molecule imaging of the oligomer formation of the nonhexameric Escherichia coli UvrD helicase. *Biophys. J.* **104**, 924–933 (2013).
85. H. Yokota, Quantitative and kinetic single-molecule analysis of DNA unwinding by Escherichia coli UvrD helicase. *Biophys. physicobiology* **19**, n/a (2022).
86. H. M. Arthur, P. B. Eastlake, Transcriptional control of the uvrD gene of Escherichia coli. *Gene* **25**, 309–316 (1983).
87. Y. Taniguchi, *et al.*, Quantifying E. coli proteome and transcriptome with single-molecule sensitivity in single cells. *Science* **329**, 533–8 (2010).
88. G. W. Li, D. Burkhardt, C. Gross, J. S. Weissman, Quantifying absolute protein synthesis rates reveals principles underlying allocation of cellular resources. *Cell* **157**, 624–635 (2014).
89. J. Atkinson, M. K. Gupta, P. McGlynn, Interaction of Rep and DnaB on DNA. *Nucleic Acids Res.* **39**, 1351–1359 (2011).
90. S. V. Rajagopala, *et al.*, The binary protein-protein interaction landscape of Escherichia coli. *Nat. Biotechnol. 2014 323* **32**, 285–290 (2014).
91. D. K. Orrens, C. P. Selbys, J. E. Hearst, A. Sancars, Post-incision Steps of Nucleotide Excision Repair in Escherichia coli DISASSEMBLY OF THE UvrBC-DNA COMPLEX BY HELICASE I1 AND DNA POLYMERASE I*. *J. Biol. Chem.* **267**, 780–788 (1992).
92. P. McGlynn, R. G. Lloyd, Modulation of RNA polymerase by (p)ppGpp reveals a RecG-dependent mechanism for replication fork progression. *Cell* **101**, 35–45 (2000).
93. Y. N. Zhou, D. J. Jin, The rpoB mutants destabilizing initiation complexes at stringently controlled promoters behave like “stringent” RNA polymerases in Escherichia coli. *Proc. Natl. Acad. Sci. U. S. A.* **95**, 2908–2913 (1998).
94. E. A. Campbell, *et al.*, Structural mechanism for rifampicin inhibition of bacterial rna polymerase. *Cell* **104**, 901–912 (2001).
95. M. Stracy, *et al.*, Live-cell superresolution microscopy reveals the organization of RNA polymerase in the bacterial nucleoid. *Proc. Natl. Acad. Sci. U. S. A.* **112**, E4390-9 (2015).
96. K. King, S. J. Benkovics, P. Modrich, Glu-11 1 Is Required for Activation of the

DNA Cleavage Center of EcoRI Endonuclease*. *J. Biol. Chem.* **264**, 11807–11815 (1989).

97. B. Nguyen, Y. Ordabayev, J. E. Sokoloski, E. Weiland, T. M. Lohman, Large domain movements upon UvrD dimerization and helicase activation. *Proc. Natl. Acad. Sci.* **114**, 12178–12183 (2017).
98. A. Wagner, Robustness against mutations in genetic networks of yeast. *Nat. Genet. 2000 244* **24**, 355–361 (2000).
99. J. Atkinson, *et al.*, Localization of an accessory helicase at the replisome is critical in sustaining efficient genome duplication. *Nucleic Acids Res.* **39**, 949–957 (2011).
100. S. C. Massoni, S. J. Sandler, Specificity in suppression of SOS expression by recA4162 and uvrD303. *DNA Repair (Amst).* **12**, 1072–1080 (2013).
101. K. H. Maslowska, K. Makiela-Dzbenska, I. J. Fijalkowska, The SOS system: A complex and tightly regulated response to DNA damage. *Environ. Mol. Mutagen.* **60**, 368–384 (2019).
102. R. C. Centore, S. J. Sandler, UvrD limits the number and intensities of RecA-green fluorescent protein structures in Escherichia coli K-12. *J. Bacteriol.* **189**, 2915–2920 (2007).
103. V. Petrova, *et al.*, Active displacement of RecA filaments by UvrD translocase activity. *Nucleic Acids Res.* **43**, 4133–4149 (2015).
104. M. M. Cox, Regulation of bacterial RecA protein function. *Crit. Rev. Biochem. Mol. Biol.* **42**, 41–63 (2007).
105. N. Raghunathan, S. Goswami, J. K. Leela, A. Pandiyan, J. Gowrishankar, A new role for Escherichia coli Dam DNA methylase in prevention of aberrant chromosomal replication. *Nucleic Acids Res.* **47**, 5698–5711 (2019).
106. H. Yokota, Roles of the C-Terminal Amino Acids of Non-Hexameric Helicases: Insights from Escherichia coli UvrD. *Int. J. Mol. Sci.* **22**, 1–19 (2021).

Supplementary Information

Tetrameric UvrD helicase is located at the *E. coli* replisome due to frequent replication blocks

Adam J. M Wollman[1,2,3,], Aisha H. Syeda[1,2], Jamieson A. L. Howard[1,2], Alex Payne-Dwyer[1,2], Andrew Leech[4] , Colin Guy[5, 6], Peter McGlynn[2,6], Michelle Hawkins[2] and Mark C. Leake[1,2]

The authors wish it to be known that, in their opinion, the first two authors should be regarded as joint First Authors

[1] School of Physics, Engineering and Technology, University of York, York YO10 5DD, United Kingdom.

[2] Department of Biology, University of York, York YO10 5DD, United Kingdom.

[3] Current address: Biosciences Institute, Newcastle University, NE1 7RU, United Kingdom.

[4] Bioscience Technology Facility, Department of Biology, University of York, York YO10 5DD, United Kingdom

[5] Current address: Covance Laboratories Ltd., Otley Road, Harrogate, HG3 1PY, United Kingdom

[6] Previous address: School of Medical Sciences, Institute of Medical Sciences, University of Aberdeen, Foresterhill, Aberdeen AB25 2ZD, United Kingdom

* To whom correspondence should be addressed. To whom correspondence should be addressed. Tel: +44 (0)1904322697. Email: mark.leake@york.ac.uk

Present Address: School of Physics, Engineering and Technology, and Department of Biology, University of York, York YO10 5DD, United Kingdom

Supplementary Tables

Table S1 Strains used in this study

Strain	Relevant genotype	Source or derivation
BW25113 derivatives:		
BW25113	*rrnB ΔlacZ4787 hsdR514 Δ(araBAD)567 Δ(rhaBAD)568 rph-1*	(1)
JW2703	*ΔmutS::<kan>*	(1)
JW3786	*ΔuvrD::<kan>*	(1)
JW4019	*ΔuvrA::<kan>*	(1)
MG1655 derivatives:		
TB12	*ΔlacIZYA::<kan>*	
TB28	*ΔlacIZYA*	(2, 3)
TB28 derivatives		
N6577	*ΔlacIZYA Δrep::cat*	(4)
N6661	*ΔlacIZYA::<> Δrep::dhfr* / pAM407 (*uvrD*$^+$ *lacZ*$^+$, a pRC7 derivative)	(4)
N6661	*ΔlacIZYA::<> Δrep::dhfr* / pAM407 (*uvrD*$^+$ *lacZ*$^+$, a pRC7 derivative)	(4)
N6644	*ΔlacIZYA::<> uvrD::dhfr Δrep::cat* / pAM407 (*uvrD*$^+$ *lacZ*$^+$, a pRC7 derivative)	(4)
JGB166	*ΔuvrD* / pKD46	JW3786 transformed with pKD46
AS97	TB28/pKD46	(5)
AS446	*dnaQ-mCherry-<kan>*	
AS448	*dnaQ-mCherry-<>*	(5)
AS512	*mGFP-uvrD-<kan>*	*mGFP-uvrD-<kan>* recombineered into JGB166
AS517	*ΔlacIZYA::<> Δrep::cat mGFP-uvrD-<kan>* / pAM407 (*uvrD*$^+$ *lacZ*$^+$, a pRC7 derivative)	N6661 X P1(AS512)
AS564	*dnaQ-mCherry-<kan> rpoB*35*	PM486 X P1(AS446)
AS571	*dnaQ-mCherry-<> rpoB*35*	AS564 to km^S with pCP20
AS580	*dnaQ-mCherry-<> mGFP-uvrD-<kan>*	AS448 X P1(AS512)
AS582	*dnaQ-mCherry-<> mGFP-uvrD-<kan> rpoB*35*	AS571 X P1(AS512)
AS590	*dnaQ-mCherry-<> mGFP-uvrD-<kan> Δrep::cat*	AS580 X P1(N6577)
AS650	*dnaQ-mCherry-<> mGFP-uvrD-<>*	AS580 to km^S with pCP20
AS656	*dnaQ-mCherry-<> mGFP-uvrD-<> ΔuvrA::<kan>*	AS650 X P1(JW4019)
AS658	*dnaQ-mCherry-<> mGFP-uvrD-<> ΔmutS::<kan>*	AS650 X P1(JW2703)

991 **Table S2 Plasmids used in this study**

Plasmid	Description	Antibiotic	Reference
pCP20	Yeast Flp recominase expression plasmid	Amp	(6)
pKD46	λ Red recombinase expression plasmid	Amp	(6)
pAS79	pUC18 *mGFP-uvrD-<kan>*	Amp, kan	This study
pAS152	pET14b-mGFP uvrD	Amp	This study

992
993

994 **Table S3 Oligonucleotides used in this study**

Primer	Sequence (5' - 3')
oJGB383	TGAATGATTTTTTAGGCCAAATAAGGTGCGCAGCACCGCATCCGGCAACGCATATGAATATCCTCCTTAG
oJGB417	TACAAGACACGTGCTGAAGTC
oJGB418	TGCTAGTTGAACGCTTCCATC
oMKG71	CGGTGCCCTGAATGAACTGC
oPM319	CTTGTTGGATCAGACCGGAAAATG
oPM320	TGGCAACGCTATCCTTTTGTCA
oPM407	GCGGCAGGCAATGTGGTA
oPM409	CCTTTGAGCGTGTGGTGA
oPM411	CAGCGGCTACAAGCTCGG
oPM187B20	GTCGGATCCTCTAGACAGC(BiodT)CCATGATCACTGGCACTGGTAGAATTCGGC
oPM188B34	AACGTCATAGACGATTACATTGCTACATGGAGC(BiodT)GTCTAGAGGATCCGAC
oAS84	CCCGTCTCGATCTGGTGCAG
oAS85	TTGCTGCAAAAATCGCCCAAG
oAS132	CCCGTCTCGATCTGGTGCAGAAGAAAGGCGGAAGTTGCCTCTGGCGAGCAGGCTGGCTCCGCTGCTGG
oAS133	TTGCTGCAAAAATCGCCCAAGTCGCTATTTTTAGCGCCTTTCACAGGTATCATATGAATATCCTCCTTAG
oAS145	AGGGCGTTGCGCTTCTCCGCCCAACCTATTTTTACGCGGCGGTGCCAATGAGTAAAGGAGAAGAACTT

995

996

997 **Table S4 Cell doubling times of labelled strains.** Values expressed are the means of three
998 independent replicates, with standard deviation and standard errors indicated.

Strain (Relevant genotype)	LB medium			Minimal medium		
	Mean doubling time (min)	SD (min)	SEM (min)	Mean doubling time (min)	SD (min)	SEM (min)
WT	23.72	1.11	0.64	62.80	17.06	9.85
dnaQ-mCherry	26.85	0.91	0.52	62.22	18.63	10.76
mGFP-uvrD	24.79	0.37	0.22	59.45	1.80	1.04
dnaQ-mCherry mGFP-uvrD	25.27	1.51	0.87	71.03	7.59	4.38
ΔmutS	24.59	0.55	0.32	107.91	13.96	8.06
ΔuvrA	27.99	0.23	0.13	92.25	5.86	3.38
*ΔrpoB*35*	33.98	0.17	0.10	83.11	30.83	17.80
Δrep	24.30	2.03	1.17	62.74	1.20	0.70
dnaQ-mCherry mGFP-uvrD ΔmutS	26.85	0.68	0.39	110.84	34.91	20.16
dnaQ-mCherry mGFP-uvrD ΔuvrA	24.13	0.56	0.33	91.80	5.18	2.99
*dnaQ-mCherry mGFP-uvrD ΔrpoB*35*	32.81	0.70	0.40	99.11	78.68	45.42
dnaQ-mCherry mGFP-uvrD Δrep	26.54	1.90	1.10	62.17	2.98	1.72

999
1000
1001
1002
1003

Supplementary figures

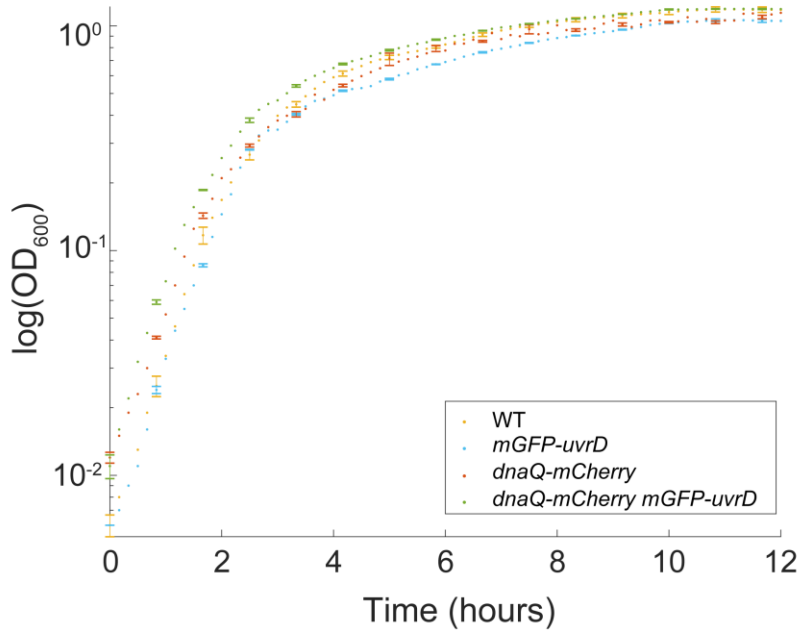

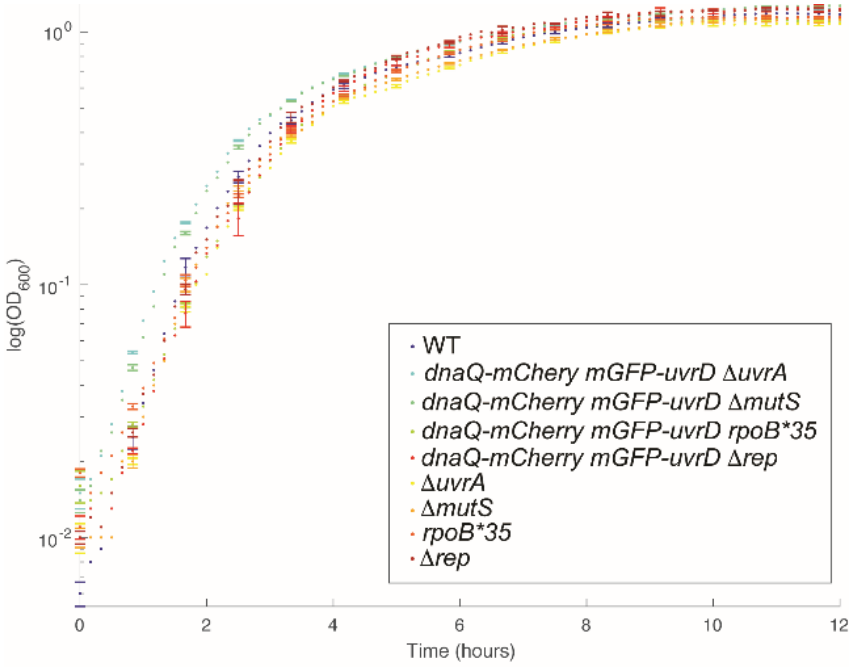

Supplementary Figure S1. Growth curves in LB medium. Cultures were grown in LB as described in the text. The OD_{600} values are plotted on a log scale on the vertical axis with a linear scale of time in hours on the horizontal axis. The genotypes of the strains are indicated in boxes within the figures. SD error bars (shown just on every 5th consecutive point for clarity here), taken from N=3 replicate cultures. Plots in panel A are growth curves of single and dual labelled wild-type strains, while those in panel B are dual labelled and unlabelled mutant strains. The unlabelled wild-type strain is included in all panels as a reference.

1016

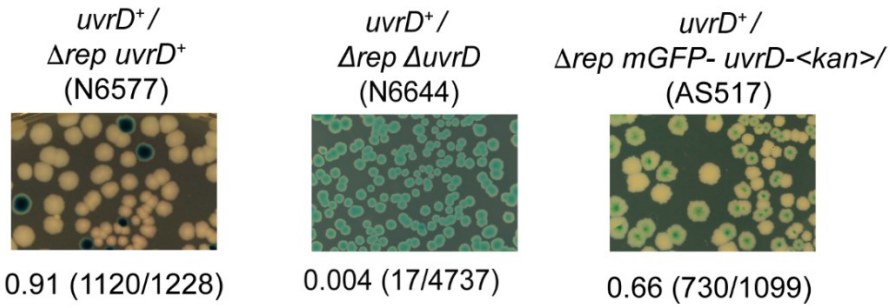

1017

1018 **Supplementary Figure S2: Testing of mGFP-UvrD fusions for retention of function.** We
1019 transformed the strain carrying a chromosomal *mGFP-uvrD* allele with a derivative of pRC7
1020 carrying a wild-type *uvrD* allele (pPM407), which is an unstable low copy plasmid that also
1021 carries the *lacZYA* genes (3). Presence of this plasmid confers blue colour to the colonies on
1022 plates containing Xgal when strains are chromosomally deleted for the *lac* operon. In rapidly
1023 growing cells, cells require either *rep* or *uvrD* for viability, and the loss of both is lethal (4, 7).
1024 Thus, *Δrep* cells with a functional *uvrD* allele are viable and can lose pRC7*uvrD*, evidenced
1025 by appearance of white colonies on LB Xgal IPTG plates, but cells lacking *uvrD* function
1026 cannot survive upon loss of the plasmid resulting in recovery of only blue colonies. The *Δrep*
1027 *mGFP-uvrD* cells produced white colonies on Xgal media, indicating that the *mGFP-uvrD*
1028 fusion is functional.

1029

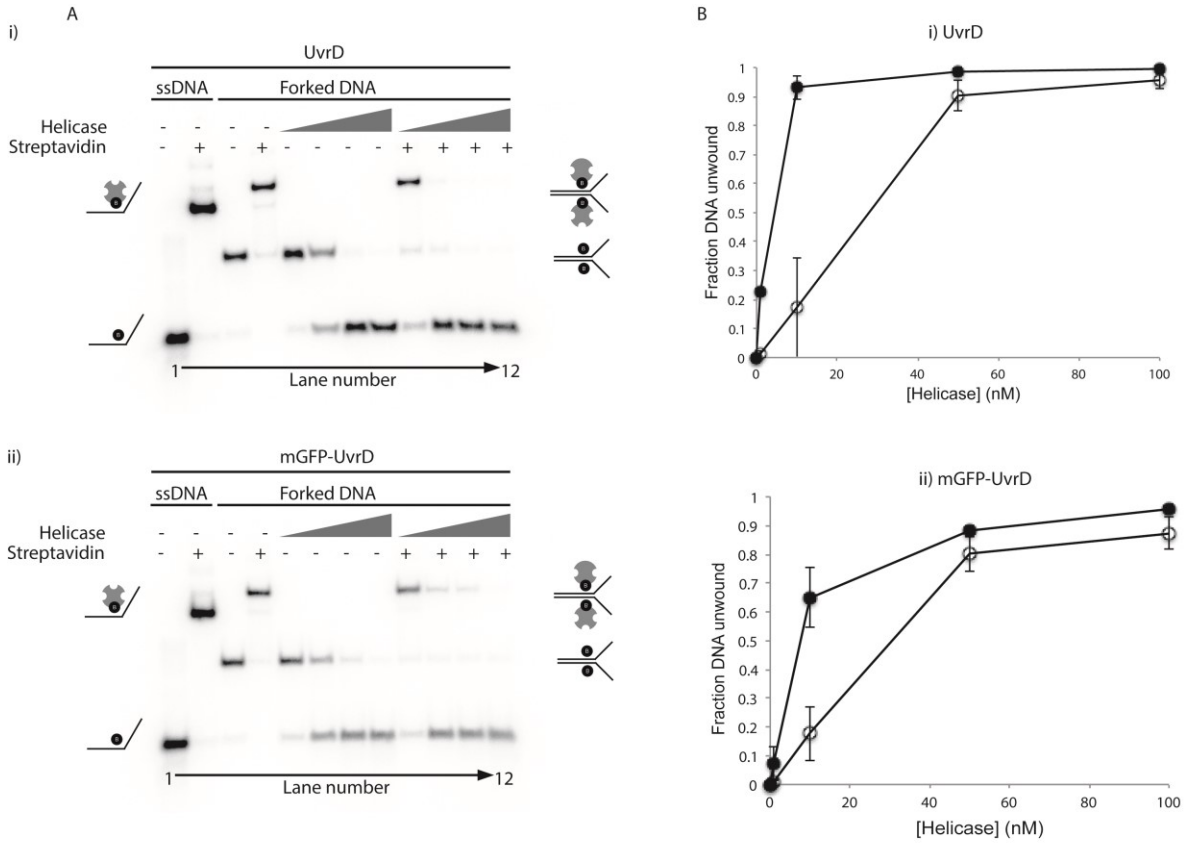

Supplementary Figure S3: mGFP-UvrD fusion is functional *in vitro*. (A) Representative native polyacrylamide TBE gels showing (i) UvrD and (ii) mGFP-UvrD unwinding of forked DNA containing biotin on both strands within the duplex region (8, 9). Lanes 1-4 contain markers indicating the position of single stranded or forked DNA +/- streptavidin as indicated. Lanes 5-12 contain the products of unwinding the forked DNA +/- streptavidin by the indicated helicase at 1, 10, 50 and 100 nM. (B) Quantification of the unwinding of the forked substrate in the absence of (open circles) and presence of (closed circles) streptavidin by the indicated helicases. Data points shown are averages of band intensities (taken from two gels in UvrD and four gels in mGFP-UvrD) with standard errors indicated by bars on the points.

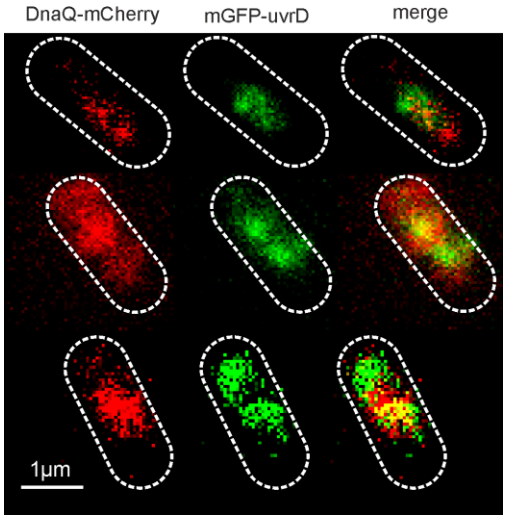

Supplementary Figure S4: Dual colour Slimfield images of mGFP-UvrD:DnaQ-mCherry, scale bar 1 micron. Segmented outlines of cell bodies indicated (white dash).

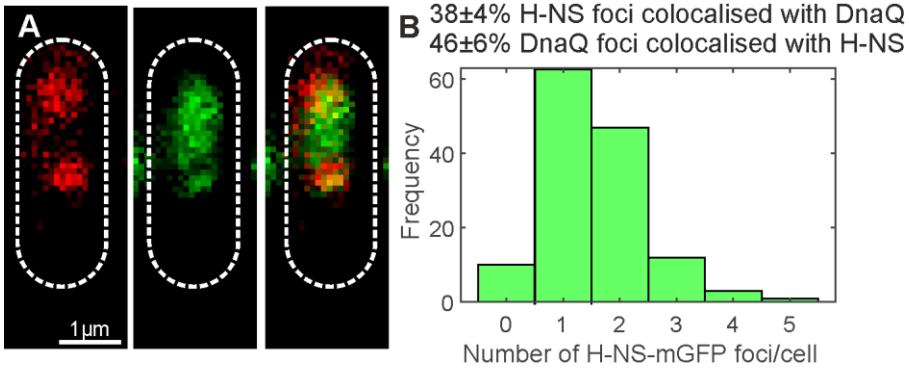

Supplementary Figure S5: (A) Dual colour Slimfield images of H-NS-mGFP-:DnaQ-mCherry, scale bar 1 micron. Segmented outlines of cell bodies indicated (white dash). (B) Histogram showing the number of H-NS foci detected per cell, SD errors.

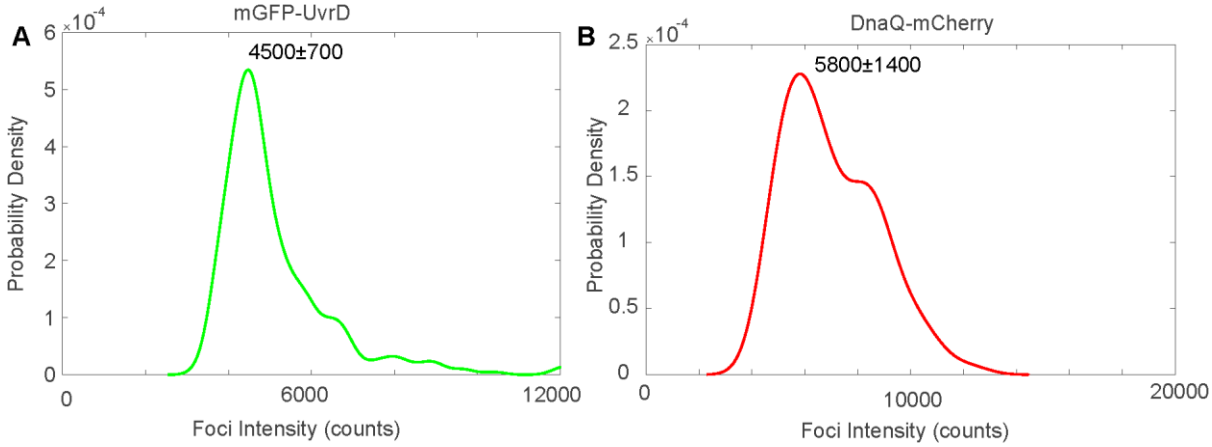

Supplementary Figure S6: Brightness of single mGFP and mCherry molecules A. and B. Characteristic intensity distributions rendered as kernel density estimates of single mGFP-UvrD and DnaQ-mCherry. Peak±full width at half maximum indicated. Distributions calculated from the tracked foci intensity distributions from the end of the photobleach process such that only single fluorophore molecules are detected. Number of molecules per foci before bleaching is determined by dividing the initial foci intensity by these values for the equivalent fluorophore.

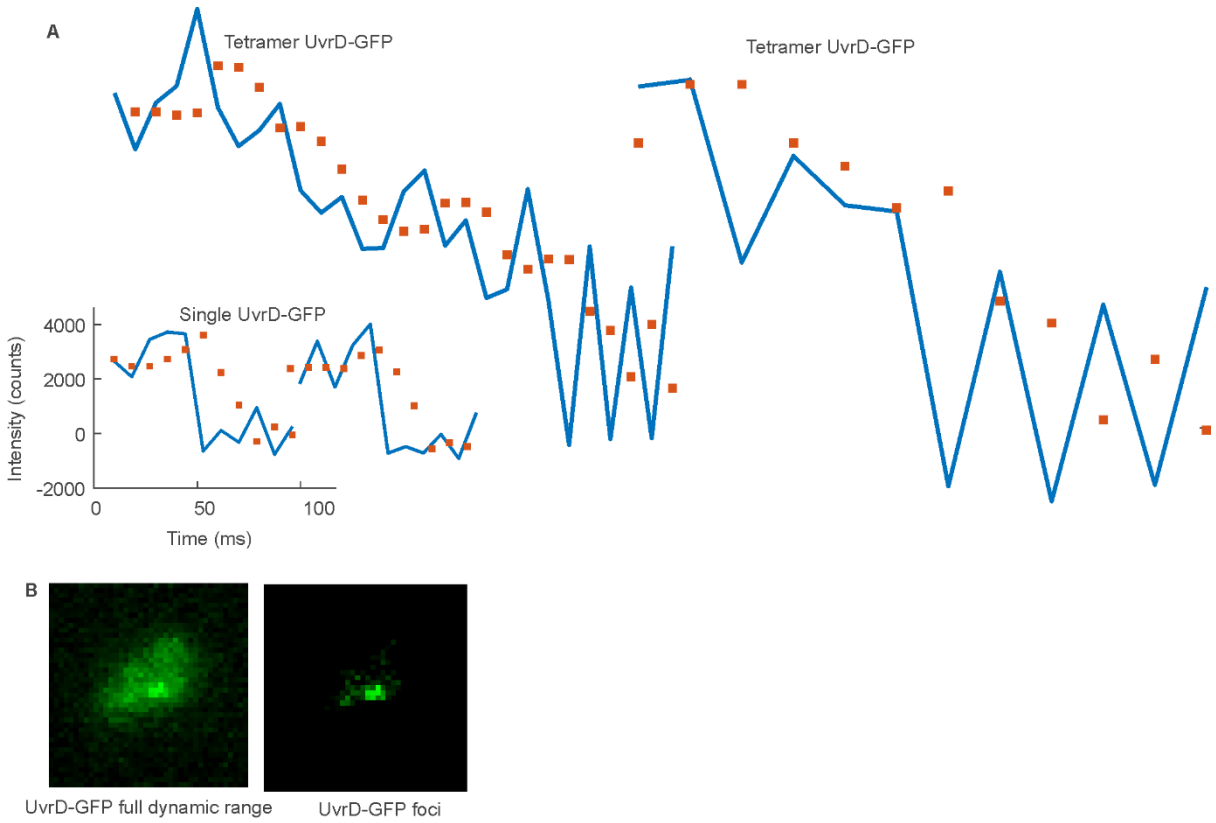

Supplementary Figure S7: Single-molecule image analysis. A. Chung-Kennedy filtered (squares) intensity traces for single UvrD tracks showing tetramers exhibiting multiple photobleach steps and monomers detected towards the end of photobleaching. Foci were 'overtracked' beyond the last detected bright frame to illustrate steps. **B**. UvrD-GFP micrograph showing the full dynamic range (left) and adjusted to illustrate a foci (right)

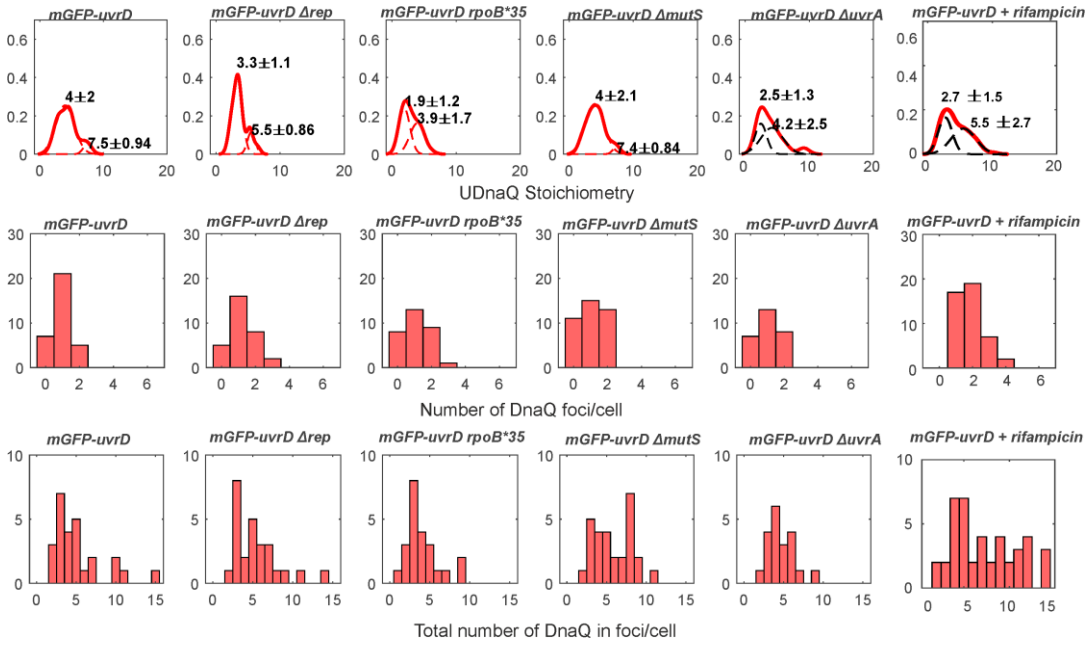

Supplementary Figure S8: DnaQ tracking characterization. Top row: Distribution of DnaQ foci stoichiometry as a kernel density estimate for all strains and conditions (red) with two Gaussian fit overlaid as black dotted lines. Peak ± half width at half maximum shown above. Middle row: Corresponding histogram of number of foci detected per cell. Bottom row: histogram of the total amount of DnaQ in foci per cell. N=30-50 cells per strain or condition.

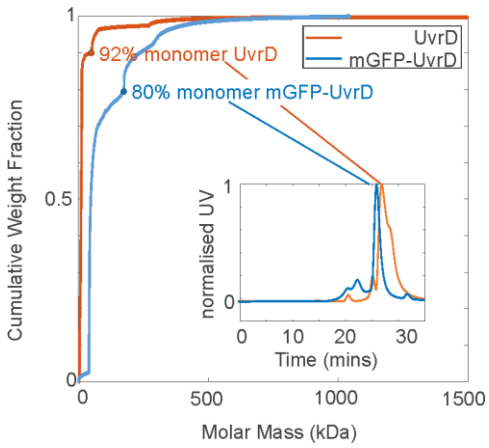

Supplementary Figure S9: SEC-MALLS of UvrD/mGFP UvrD . Size Exclusion Chromatography - Multi-Angle Laser Light Scattering (SEC-MALLS) of 4μM UvrD (red) and mGFP-UvrD (blue) cumulative weight fraction as a function of molar mass. 92% of UvrD and 80% of mGFP-UvrD is consistent with a monomer. Inset shows the normalised UV abosorbance as a function of elution time through the column with the monomer peaks indicated.

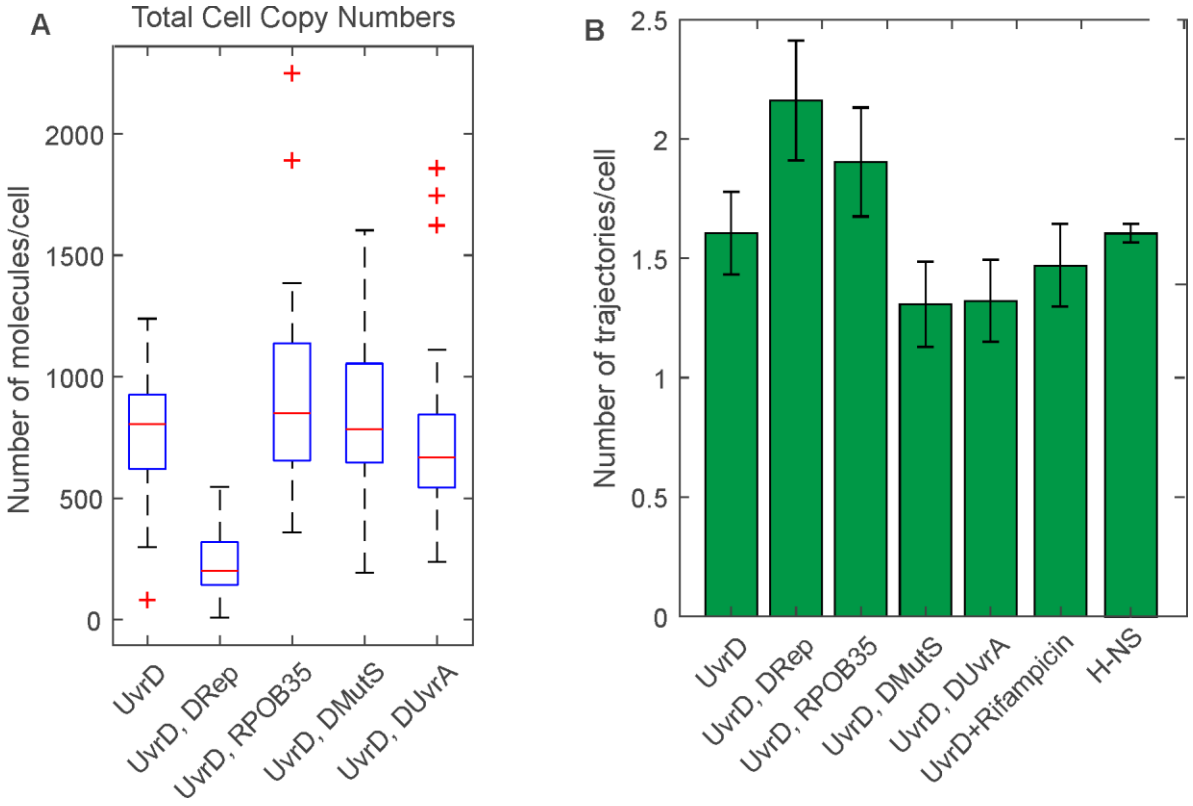

Supplementary Figure S10: A. Boxplot of the total number of mGFP-UvrD molecules per cell, estimated by numerical integration of the whole cell fluorescence. Median is shown as red line, bottom and top of the blue box mark the 25th and 75th percentiles and whiskers extend to the most extreme points not considered outliers (2.7 standard deviations covering 99.3% of normally distributed data) with outliers beyond this shown as red +. N=30 cells per strain. B Number of trajectories per cell used in the stoichiometry determination

1098

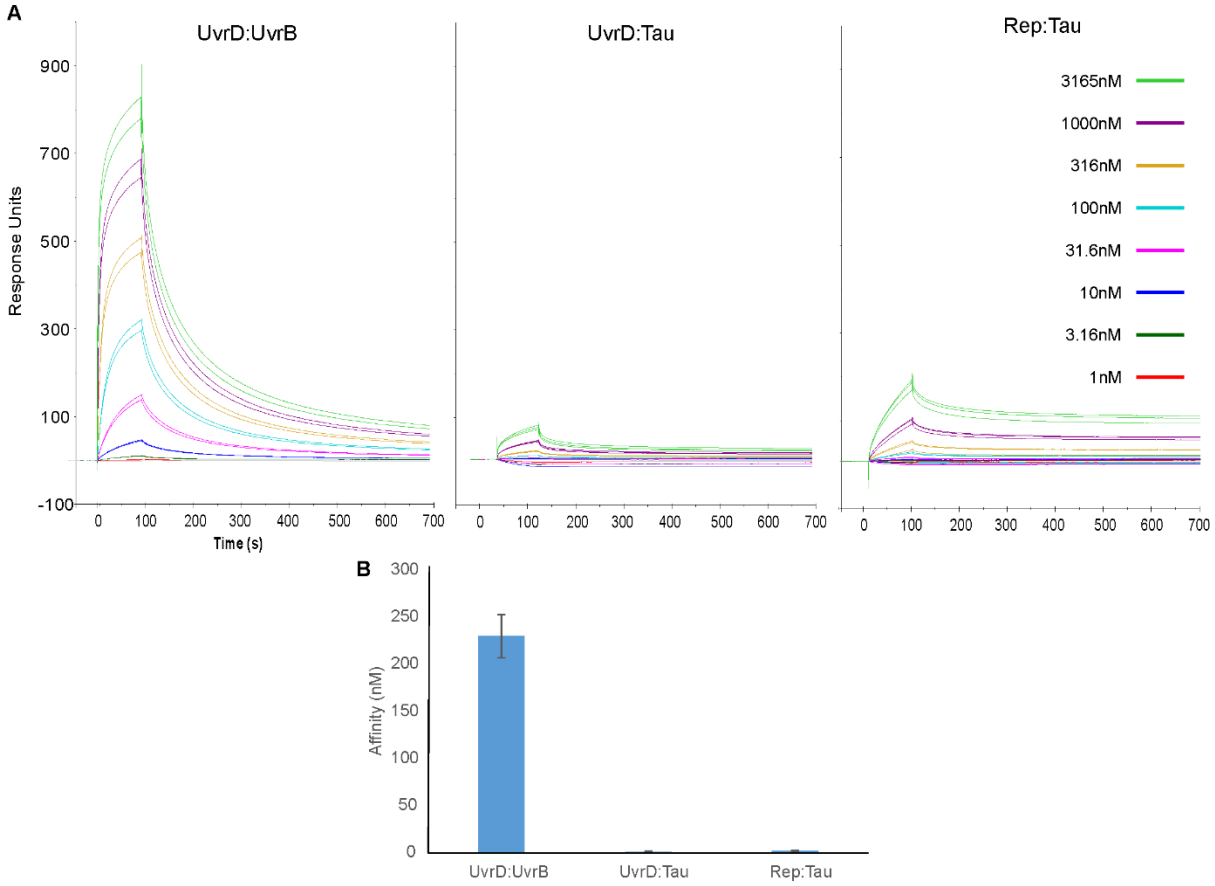

1099

1100 **Supplementary Figure S11: Surface plasmon resonance measurements of helicase**
1101 **interactions with Tau** A. Titration response curves for UvrD:UvrB, UvrD:Tau and Rep:Tau
1102 with their affinities shown in B.

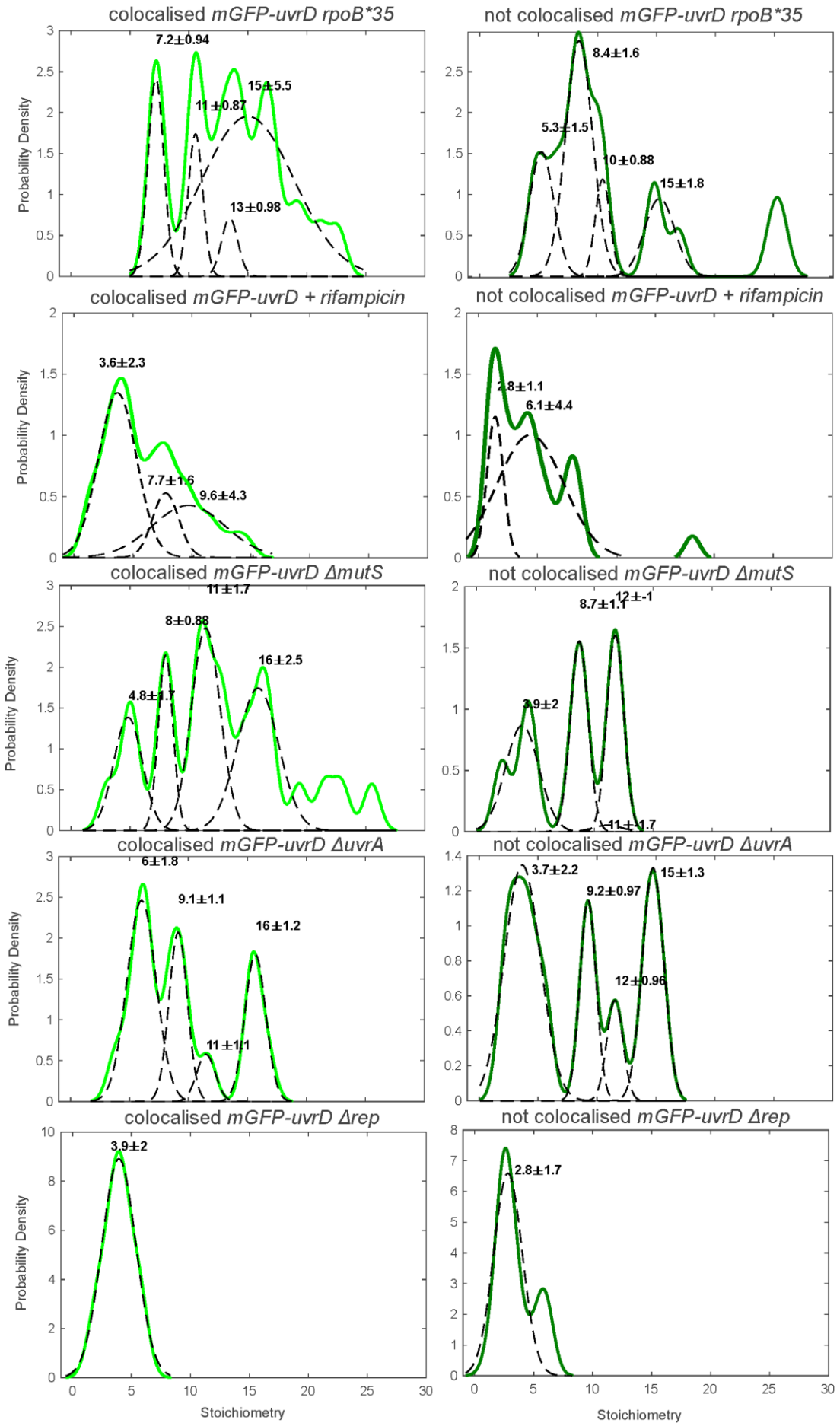

1103

Supplementary Figure S12: Perturbed UvrD stoichiometry. The distribution of UvrD foci stoichiometry rendered as a kernel density estimate for foci colocalised (Left) and non-colocalised (Right) with DnaQ foci. Distributions were fitted with multiple Gaussian fits (black dotted lines) with the peak value ± half width at half maximum indicated above each peak.

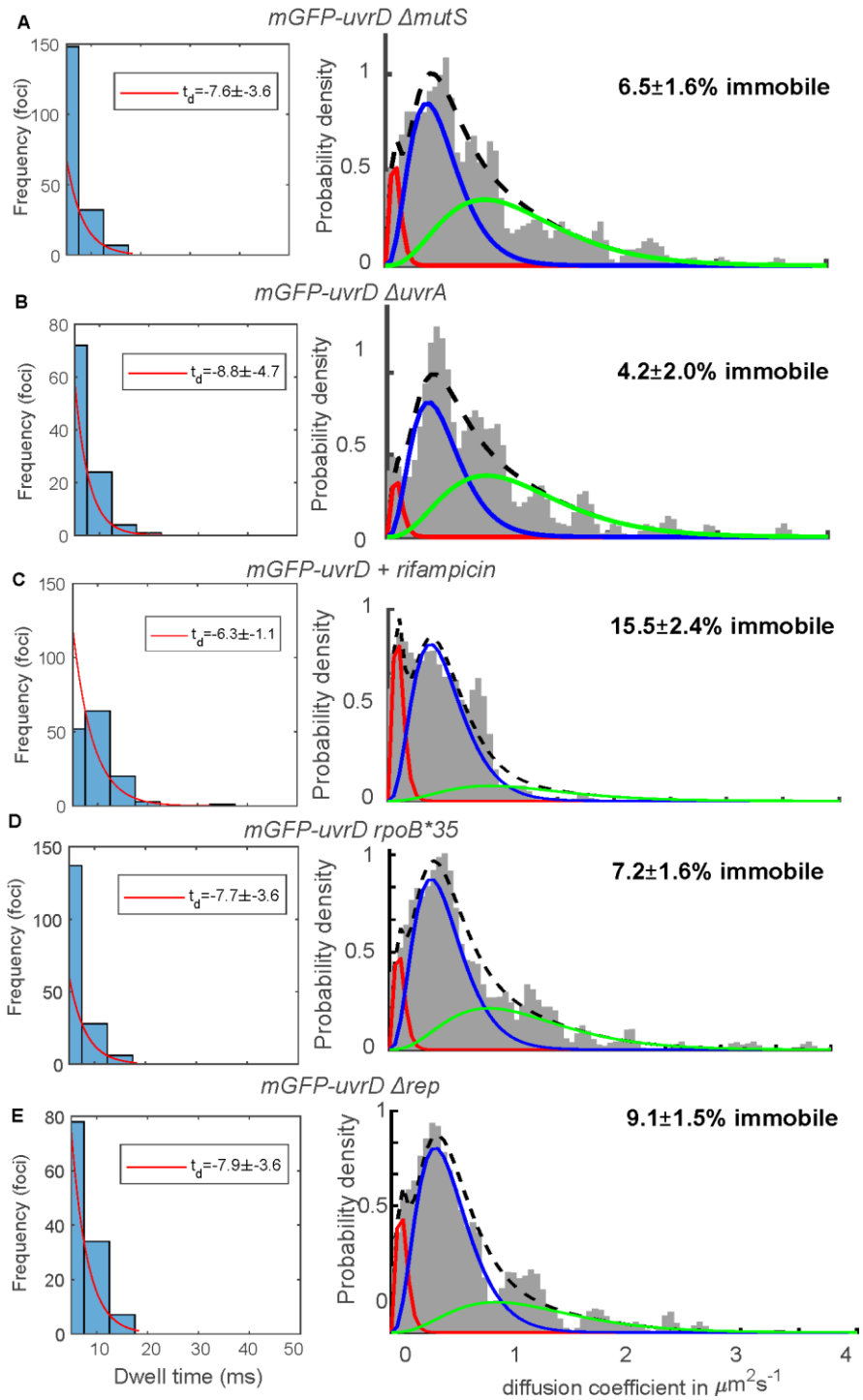

Supplementary Figure S13: UvrD perturbed dynamics. A-E Left, distribution of time UvrD and DnaQ foci were colocalised (blue) fit with an exponential (red) to yield a characteristic dwell time. Right, distribution of microscopic diffusion coefficients of UvrD foci (grey) fitted with a three state gamma distribution model containing a relatively immobile population with D = 0.1 μm²/s (red), a transiently immobile population, D = 0.5 μm²/s (blue) and a mobile population, D=1.2 μm²/s (green). Errors represent 95% confidence intervals. N~300 foci/condition.

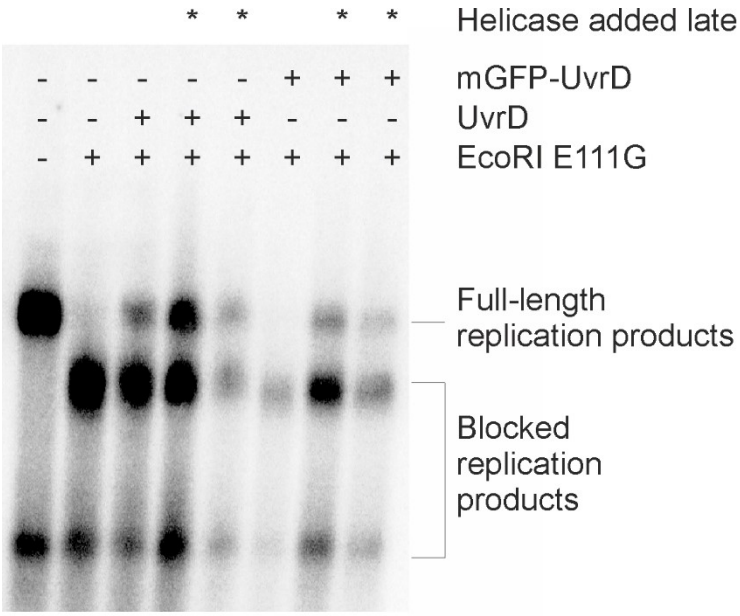

Supplementary Figure S14: In vitro replication assay using mGFP-UvrD. Denaturing agarose gel of replication products formed from pPM872 (1) in the absence and presence of EcoRI E111G block, mGFP-UvrD and UvrD added pre- and post-collision (*) as indicated.

Supplementary references

1. Baba,T., Ara,T., Hasegawa,M., Takai,Y., Okumura,Y., Baba,M., Datsenko,K.A., Tomita,M., Wanner,B.L. and Mori,H. (2006) Construction of Escherichia coli K-12 in-frame, single-gene knockout mutants: the Keio collection. *Mol. Syst. Biol.*, **2**, 2006.0008.
2. Bachmann,B.J. (1996) Derivations and genotypes of some mutant derivatives of Escherichia coli K-12. . In Neidhardt,F.C., Curtiss III,R., Ingraham,J.L., Lin,E.C.C., Low,K.B., Magasanik,B., Reznikoff,W.S., Riley,M., Schaechter,M., Umbarger,H.E. (eds), *Escherichia coli and Salmonella cellular and molecular biology*. ASM Press, Washington, DC, pp. 2460–2488.
3. Bernhardt,T.G. and de Boer,P.A.J. (2004) Screening for synthetic lethal mutants in Escherichia coli and identification of EnvC (YibP) as a periplasmic septal ring factor with murein hydrolase activity. *Mol. Microbiol.*, **52**, 1255–1269.
4. Guy,C.P., Atkinson,J., Gupta,M.K., Mahdi,A.A., Gwynn,E.J., Rudolph,C.J., Moon,P.B., van Knippenberg,I.C., Cadman,C.J., Dillingham,M.S., *et al.* (2009) Rep provides a second motor at the replisome to promote duplication of protein-bound DNA. *Mol. Cell*, **36**, 654–666.
5. Syeda,A.H., Wollman,A.J.M., Hargreaves,A.L., Howard,J.A.L., Brüning,J.-G., McGlynn,P. and Leake,M.C. (2019) Single-molecule live cell imaging of Rep reveals the dynamic interplay between an accessory replicative helicase and the replisome. *Nucleic Acids Res.*, **47**, 6287–6298.
6. Datsenko,K.A. and Wanner,B.L. (2000) One-step inactivation of chromosomal genes in *Escherichia coli* K-12 using PCR products. *Proc. Natl. Acad. Sci. USA*, **97**, 6640–6645.
7. Boubakri,H., de Septenville,A.L., Viguera,E. and Michel,B. (2010) The helicases DinG, Rep and UvrD cooperate to promote replication across transcription units in vivo. *EMBO J.*, **29**, 145–157.
8. Brüning,J.-G., Howard,J.A.L. and McGlynn,P. (2016) Use of streptavidin bound to biotinylated DNA structures as model substrates for analysis of nucleoprotein complex disruption by helicases. *Methods*, **108**, 48–55.
9. Brüning,J.-G., Howard,J.A.L., Myka,K.K., Dillingham,M.S. and McGlynn,P. (2018) The 2B subdomain of Rep helicase links translocation along DNA with protein displacement. *Nucleic Acids Res.*, **46**, 8917–8925.